NITROGEN IN SL/RN DIRECT REDUCED IRON: ORIGIN AND EFFECT ON THE ELECTRIC STEELMAKING PROCESS

By

Markus Wouter Erwee

Submitted in partial fulfilment of the requirements

for the degree:

M.Eng (Metallurgical Engineering)

In the Department of Materials Science and Metallurgical Engineering,

Faculty of Engineering, the Built Environment and Information Technology, University of Pretoria, Pretoria, South Africa.

October, 2013

Abstract

NITROGEN IN SL/RN DIRECT REDUCED IRON: ORIGIN AND EFFECT ON THE ELECTRIC STEELMAKING PROCESS

Candidate : Markus Wouter Erwee

Supervisor : Professor P.C. Pistorius

Department : Materials Science and Metallurgical Engineering

Degree : Master of Engineering (Metallurgical Engineering)

Direct Reduced Iron (DRI) is used as an alternative feedstock in electric arc furnaces, making up 50% or more of the total iron charge. DRI produced with coal based reductants (for example in rotary kilns) make up roughly 25% of DRI produced in the world. It was found that SL/RN DRI samples from a kiln cooler had high nitrogen contents (50-250ppm, depending on particle size), higher than DRI from gas-based reduction. The higher nitrogen content of SL/RN DRI would increase the levels of nitrogen of liquid steel produced in the EAFs. The problem is exacerbated by the fact that the SL/RN DRI contains virtually no carbon (which would aid in preventing nitrogen pickup). The proposed mechanism of nitrogen pick-up by the SL/RN DRI is one where nitrogen present within the atmosphere of the rotary cooler (where hot DRI, discharged at 1000°C from the rotary kiln, is cooled to approximately 100 °C in ca. two hours) penetrates the solids bed and nitrides DRI particles. Possible rate-determining steps for nitriding in the cooler have been evaluated. Nitriding of DRI particles is predicted to be rapid: the most plausible location for rapid nitrogen pickup is the first 5 meters of the rotary cooler, where the high temperature, nitrogen-rich gas atmosphere and rapid solids bed mixing are conducive to nitriding; solid-state and pore diffusion of nitrogen into DRI particles are predicted to be rapid too. The most plausible rate determining step for nitriding of DRI particles is that of nitrogen dissociation on the DRI surface, which can be further retarded by the presence of sulphur. A strong correlation was found between the amount of "melt-in" carbon in the liquid steel and the final tap nitrogen content, with 0.3% C resulting in nitrogen levels as low as 50 ppm (80 ppm or less is desired on the plant in question) at tap, even with DRI material that is high in nitrogen and contains virtually no carbon. Proposals to increase the melt-in carbon are included.

Keywords: Direct Reduced Iron (DRI), Electric Arc Furnace Steelmaking, Nitrogen, SL/RN DRI, nitriding, dusty-gas model

Table of Contents

Acknowledgements

I would like to express my gratitude and appreciation to the following people, institutions and companies for support and assistance during the course of this project:

- My supervisor, Prof. Chris Pistorius for his supervision, everlasting patience, insight, support and advice, throughout this project and my career thus far – the value of having a mentor like him cannot be overstated and his wife Sharon, for encouragement;
- My late grandmother, for her support and sacrifice throughout my life and especially for the inspiration she was to me and her confidence in me;
- My cousin, William, who never gave up on me and helped out with all the hard physical work;
- My closest, loyal friends: Stefan (for always being firm, yet gentle and inspiring when I needed it most and never giving up on me), Sarah Havenga and Madeleine du Toit (for always having my back and always believing in me and also being an inspiration to me), Jolandie (for comfort when I needed a break from it all), Pieter (for pushing me to finish more than once and being firm when needed), Dewald, Andri, Nelis, Joalet, Getrude, Gavin, Henri, James, Rossouw, Elzaan and Horisane (for never doubting that I would finish and always understanding that I need some time to work on this project!). To all of you: Thank you for suffering through this with me;
- Also to my colleagues: Louise Ackermann, Johan de Villiers & Andrie Garbers-Craig, Izette Willemse, Liz Jones, Luzaan , Louise B, Jenny for their encouragement;
- To Dr Johan Zietsman and Dr Robert Cromarty for their contribution in encouraging me to finish;
- Ntkateko Mhlongo, Johan Terblanche, Roelf Janse van Rensburg, Alex Horne, Erwee Lourens, Matthews Khetane and Johann Petrick from ArcelorMittal Vanderbijlpark for samples, data and many e-mails;
- The Department of Materials Science and Metallurgical Engineering, University of Pretoria for financial support;
- To each and every person that has ever asked me "How's your project going?" and I did not mention in this section.

"The only real failure is the failure to try and the measure of success is how we cope with disappointment. As we always must. We came here and we tried. All of us in our different ways. Can we be blamed for feeling that we are too old to change? Too scared of disappointment to start it all again? We get up in the morning, we do our best. Nothing else matters. But it is also true that the person who risks nothing, does nothing, has nothing. All we know about the future is that it will be different. But perhaps what we fear is that it will be the same. So we must celebrate the changes because as someone once said: everything will be alright in the end and if it's not alright, then trust me, it's not yet the end." – Quote from "The Best Exotic Marigold Hotel", based on the book "These Foolish Things" by Deborah Moggach.

Chapter 1:
Introduction

Direct reduced iron (DRI) has become a valuable iron feedstock for the electric arc furnace (EAF). EAF steelmaking remains popular and continues to grow due to the cost and environmental advantages compared with, for example, the blast furnace-BOF route[1]. Referring to DRI as a secondary iron unit would at this moment in time be slightly incorrect, as many producers charge in excess of 50% of the total iron input into EAF units. The replacement of expensive scrap with this virgin iron unit has become very popular: an analogy can be drawn between the replacement of scrap with DRI in the EAF as iron ore (etc.) was replaced with sinter in the blast furnace with time. Growth in the production of DRI has been substantial in the last 40 years, worldwide. Up to the year 2010, worldwide production of DRI has increased by ca. 60% to 70.37 Mt[2]. Recent figures are similar (the top 11 countries producing DRI produced roughly 55 Mt in 2012 based on the assumption that these countries accounted for 82% of the total DRI produced in the world in 2012[3]).

DRI production is dominated by gas-based reductant processes like MIDREX (producing ca. 58% of the total DRI worldwide in 2010), but coal-based reduction remains an integral part of the market in both India and South Africa – where coal is relatively cheap and gaseous reductants are not readily available. In total, approximately 25% of DRI is produced in coal-based reductant processes[2], one of which is the Stelco-Lurgi/Republic-National (SL/RN) rotary kiln process. In 2010, this process produced 2.5% of total DRI worldwide, primarily in India and secondly in South Africa (specifically at ArcelorMittal, Vanderbijlpark).

The technical success of using DRI as an alternative iron source and the high price of steel scrap prompted ArcelorMittal South Africa (Vanderbijlpark plant) to build two additional SL/RN kilns, adding to the liquid steel capacity of the plant (ca. 250 kt/a added capacity). The DRI plant at ArcelorMittal Vanderbijlpark continues to produce, even with the EAFs currently not in operation (essential maintenance is required) – other plants are currently charging this material to EAFs.

1.1. Background to the problem and scope of the project

One particular advantage of using DRI as EAF feedstock is that lower nitrogen levels can be achieved in the liquid steel produced in the EAF (and ultimately the steel product). However, on this particular plant it was found that the nitrogen content of liquid steel tapped was higher than expected (compared with plants using DRI produced via other alternative ironmaking routes, e.g. MIDREX DRI). Levels in excess of the desired 80 ppm N were experienced at tap, which prompted further

investigation. Excessive nitrogen levels are to the detriment of the mechanical properties of the final steel product.

The purpose and scope of this project was to:

1. Understand the effect of nitrogen on the mechanical properties of steel (Chapter 2);
2. Understand the underlying mechanisms of nitrogen pickup during the EAF steelmaking process as well as what current strategies are to lessen the effect thereof (this was done by evaluation of known literature on the thermodynamics and kinetics of nitrogen pickup by steel; Chapter 3);
3. Evaluate the possibility that DRI particles produced in a SL/RN rotary kiln process contains nitrogen and that this nitrogen leads to increased nitrogen levels in liquid steel at tap. (Chapter 4);
4. Evaluate the mechanism of nitrogen pickup by DRI particles in the kiln and cooler unit by describing it mathematically and determine the most plausible rate limiting step for nitriding of particles (Chapter 5);
5. Evaluate (statistically and fundamentally) the relationship between melt carbon content in the initial melting period on the final tap nitrogen content of liquid steel. This was done (inter alia) to assess the claim that nitrogen levels can be lowered (and predicted) when the carbon content in the melt is controlled (Chapter 6);

Chapter 7 concludes the work. Recommendations are made regarding further work to counter the effect of nitrogen in SL/RN DRI on EAF operations.

1.2. Publications produced from this work

1. Erwee, M.W. and Pistorius, P.C., "Nitrogen in SL/RN Direct Reduced Iron: Origin and Effect on the Electric Steelmaking Process", AISTech 2011, 5-6 May 2011, Indianapolis, Indiana, USA (Presentation only; based on Chapters 2, 4&5).
2. Erwee, M.W. and Pistorius, P.C., "Nitrogen in SL/RN Direct Reduced Iron: Origin and Effect on the Electric Steelmaking Process", Ironmaking and Steelmaking, vol. 39, no 5, 2012, pp. 336-341. (Based on most of the work – Ch 4, parts of 5, 6 and Appendix A.1).

Chapter 2:
Nitrogen in steel:
Effect on room temperature properties

In this section, the effect of nitrogen on the mechanical properties of steel at room temperature is reviewed briefly, to stress the importance of controlling the nitrogen content of steel during steelmaking.

Nitrogen, like carbon, dissolves interstitially in α-iron. The radius of the interstitial sites in BCC iron (ferrite) is 0.019 nm (for the octahedral sites where interstitials dissolve); whilst in FCC iron (austenite) the radius is 0.052 nm. Nitrogen has an atomic radius of 0.07 nm and hence dissolution of nitrogen in the iron lattice causes lattice strain. Relaxation of this strain can be achieved by the diffusion of nitrogen atoms to lattice defects, e.g. dislocations, which causes dislocation pinning, and strain aging in plastically deformed material. The greater solubility of nitrogen in iron at low temperatures (typically below 100°C), compared with carbon, is the principal cause of strain aging of low carbon steels[4].

Strain aging is defined as the change in mechanical properties (increased yield stress) after plastic deformation due to the interactions occurring between mostly interstitial atoms (e.g. C, N) and lattice defects. It is divided into static aging (occurring after plastic deformation) and dynamic strain aging (concurrent with plastic deformation)[4].

The mechanism of strain aging was defined by Cottrell and Bilby in 1949. Essentially, the mechanism is as follows, as described by Leslie[4]:

At low temperatures (below 100°C, where the solubility of carbon is too low to have a significant effect on strain aging), some nitrogen remains in interstitial solution in the iron lattice. A stress field is present within the lattice around the nitrogen atom. To relax the stress, the nitrogen atom moves to a defect in the lattice, e.g. a dislocation, forming a "Cottrell atmosphere". The defect is then "pinned" (i.e. its movement is inhibited) by the nitrogen atom. The inhibition of movement of this defect results in a higher stress being required for plastic deformation in the material. On a load-elongation curve, the material will show an increased yield point after initial strain. The practical implication of this is that a higher stress will be required to form the steel product. Strain aging also leads to discontinuous yielding when the material is deformed and the resulting surface will show striations (called Lüders bands), which are not always aesthetically or mechanically acceptable.

Figure 2.1 shows a load-elongation curve on which the increased yield point phenomenon is shown. Note that in reality the load-elongation curve in the Lüders region (the line shown as e_L) will not be a simple straight line, but rather an oscillating one, due to the discontinuous yielding of the material. Figure 2.2 illustrates the appearance of the Lüders bands.

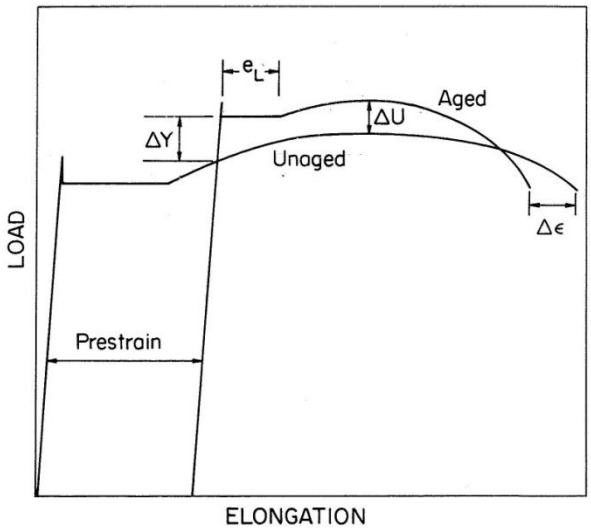

Figure 2.1: Load-elongation curve for a material that experienced static strain aging. ΔY = change in yield stress due to strain aging, e_L = Lüders strain after strain aging, ΔU = increase in ultimate tensile strength due to strain aging, Δε = decrease in elongation due to strain aging[4].

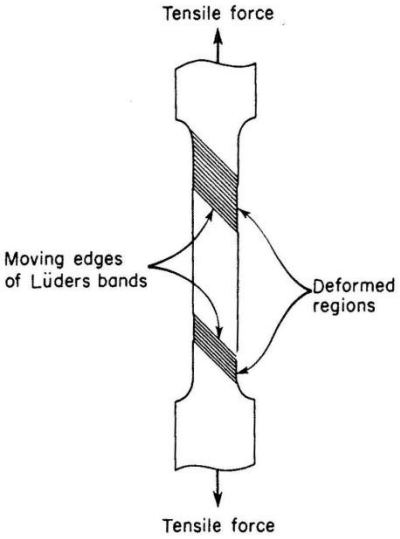

Figure 2.2: The appearance of Lüders bands in a material due to strain aging[4].

Although the interstitial dissolution of nitrogen causes a strengthening effect in steel, discontinuous yielding is detrimental. In general, sheet products are less formable and have lower toughness due to the presence of nitrogen in steel. To counter this effect, steelmakers make additions to the steel melt to limit the amount of "free nitrogen", i.e. interstitially dissolved nitrogen, in the final steel product. The amount of "free nitrogen" has a significant impact on the yield strength and formability (expressed as the mean plastic strain ratio, $\bar{r}$). A higher value of $\bar{r}$ indicates that the material is more formable – e.g. for deep drawing purposes this ratio is extremely important, since it gives the ratio of the strain in the width direction relative to the strain in the thickness direction, during tensile deformation. A higher value of $\bar{r}$ hence means a greater resistance to thinning. The effects of nitrogen in solution on the yield strength and strain ratio of steel are shown in Figures 2.3 and 2.4. Llewellyn[5] reports the Irvine relationships between the yield stress and free nitrogen ($\Delta YS \propto \%N_{soluble}$) and between the impact transition temperature ($\Delta ITT \propto \sqrt{\%N_{soluble}}$).

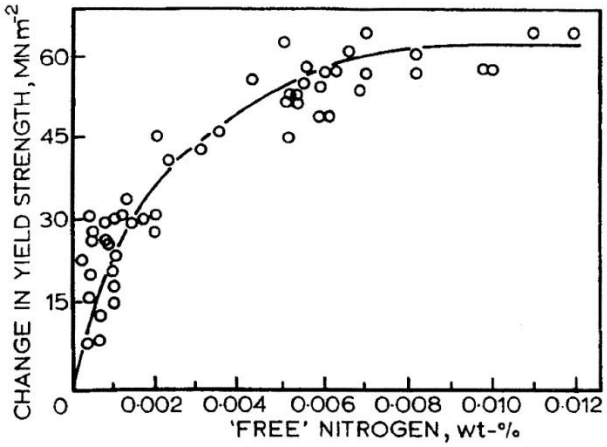

Figure 2.3: Influence of the free nitrogen content of steel on the change in yield strength (i.e. the magnitude of strain aging)[6].

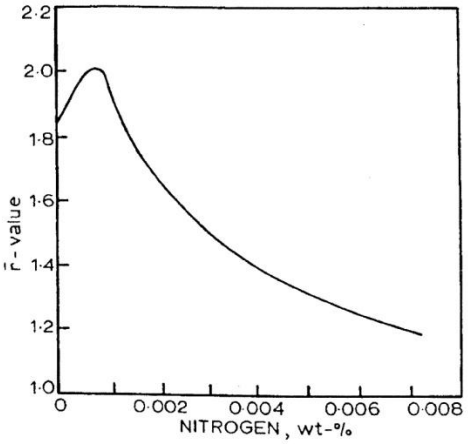

Figure 2.4: Effect of nitrogen content of steel on the mean plastic strain ratio (formability) of unkilled steels[6].

To counteract the effect of strain aging the amount of free nitrogen in steel is frequently reduced by the addition of Al to form AlN. The precipitation of AlN, in addition to reducing the amount of free nitrogen present in the steel, may also impart special properties, depending on subsequent heat treatment of the steel. By controlling the cooling rate after re-heating a low carbon steel to a typical re-heating temperature of 1250 °C, the precipitation of AlN can be controlled.

Llewellyn[5] reviewed several effects of nitrogen in steel, including the effect of cooling rate on the precipitation behaviour of AlN and the effect thereof on the mechanical properties of steel. In addition, many other authors[e.g. 6,7,8] have noted that the amount of nitrogen should be carefully controlled to control the amount of AlN that precipitates – the aim is to avoid the deleterious effects of AlN precipitation while retaining its the strengthening effect. Two major methods to control AlN precipitation are as follows:

1. Cool the steel from the reheating temperature to around 700°C, and hold it at 700°C to allow AlN precipitation. The precipitation of AlN results in low amounts of free, interstitial nitrogen at room temperature, making the material much easier to cold work. For hot ductility (important during continuous casting), the precipitation of AlN is problematic – the AlN precipitates on the austenite grain boundaries, pinning them and hence restricting relaxation of the material which in turn can cause cracking. This problem has been overcome by the addition of Ti.

2. Rapid cooling of the steel slab to a temperature in the region of 560°C after reheating suppresses formation of AlN and a significant amount of N remains in solution. Alternatively, re-heating rapidly (e.g. as in continuous annealing) to a temperature between 700 and 850°C will also result in little AlN formation. Treatment with B or Ti, resulting in the formation of nitrides at high temperatures (higher temperature than for the formation of AlN) would result in steel with high formability since no AlN is present (e.g. in "interstitial free steels", which also have low carbon contents).

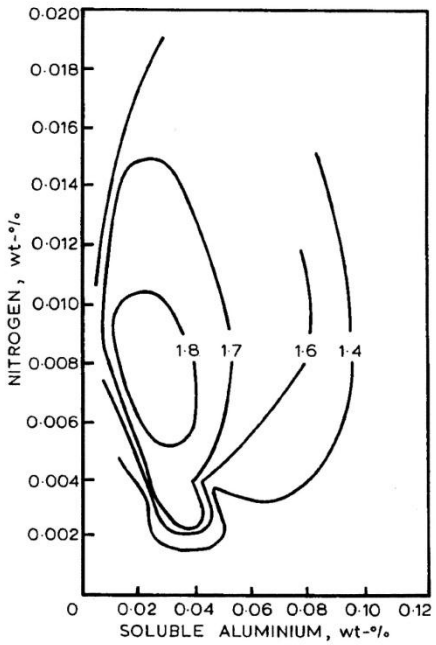

Figure 2.5 (left) shows the effect of the relative amounts of aluminium and nitrogen on the $\bar{r}$ value of a batch annealed steel sheet. The importance of careful control of the steel chemistry during steelmaking cannot be overemphasised as is shown by the effects of small differences in composition[6].

AlN is only one of the possible nitrides which are used in the manipulation of the mechanical properties of steel. Other nitrides, such as VN, TiN, BN and various carbo-nitrides (e.g. Nb(C,N), V(C,N)) can also precipitate, affecting various mechanical properties of the steel product. When little Al (≤0.02%) is present, and if V is present, VN will precipitate and a finer grain size will be achieved in structural steels[5]. In engineering steels, the use of Ti and V is common to achieve high tensile strengths, but - to retain formability - a balance between the amount of nitrogen, titanium and vanadium is required, since precipitation of too much V(C,N) could lead to less dispersion strengthening, whilst precipitation of too much TiN could lead to less dissolved interstitial nitrogen, which results in lower yield strength. Manipulation of the nitrogen content (keeping the amount of free nitrogen after TiN precipitation above 60 ppm) when using V and Ti results in the highest yield stress, whilst retaining optimum formability[5].

The use of nitrogen (and by implication the need for the careful control of the nitrogen content of steel) is not limited to the precipitation of nitrides within the structure. Tool steels and steels in which abrasion / wear resistance is most important, whilst retaining ductility (e.g. automotive transmission gears) are often nitrided or carbo-nitrided. By nitriding the surface of the component, the outer "shell" of the component becomes extremely hard and has a high resistance to wear and fatigue, whilst the ductility of the remaining (core) material is retained.

Finally, while stainless steel is *not* the focus of this dissertation it is worth mentioning that nitrogen is often used as an alloying element in stainless steels, with the following effects (based on the reviews of Llewellyn[5], Morrison[6] and Bazaleeva[9]):

- Nitrogen is a strong austenite former and hence can replace some Ni in austenitic steels – 0.35% nitrogen can replace approximately 10% Ni – although Ni imparts other beneficial properties to steel, hence it is not replaced completely;
- Nitrogen improves the pitting corrosion resistance of austenitic and duplex stainless steels and also retards sensitisation to inter-granular attack;
- Nitrogen has a strong influence on the tempering behaviour of martensitic stainless steel (since it stabilises austenite);
- Nitrogen has a solid-solution hardening effect on austenitic and duplex stainless steel grades;
- Nitrogen and carbon have very low solubility in ferritic stainless steels and must be controlled to low levels in these steels.

In conclusion – one must recognise that the nitrogen content of steel has a strong influence on the mechanical properties of steel. It is therefore, critically important that the nitrogen content of the steel be controlled during liquid steelmaking, ladle treatment, ladle transfers and casting in whichever way possible (this is discussed later in this dissertation). It is the responsibility of steelmakers to ensure this and they should use all the technology, research and experience available to achieve this. For example, Croft[8], amongst many other authors, states that "the most effective method of reducing the AlN levels in steel castings is shown to be the close control of the nitrogen content". The starting point of the steelmaker should ideally be to optimise the raw material mix for the steel to be produced, which is discussed in the next chapter on the control of nitrogen during steelmaking.

Chapter 3:
Nitrogen in liquid steelmaking

Nitrogen readily dissolves into liquid steel at steelmaking temperatures (~1600 °C). This chapter addresses the thermodynamics and kinetics of nitrogen dissolution into liquid steel (for background only; the focus of this study is mostly on *how* and *to which extent* nitrogen occurs in SL/RN DRI and what the effect of the elevated levels are on the EAF steelmaking process, rather than how it is removed).

3.1. Thermodynamics of nitrogen dissolution into iron

In order to understand why nitrogen dissolves into steel in the first place it is important to look at the solubility thereof in liquid steel. Although kinetics govern the dissolution of nitrogen (see section 3.2), it is important to understand which factors influence the equilibrium solubility of nitrogen in iron (steel should be considered as a dilute iron alloy in this case). The composition of the furnace/ladle (or subsequent steelmaking vessel) atmosphere, temperature and steel composition influence the solubility of nitrogen in iron.

Under equilibrium conditions, nitrogen can dissolve into iron according to reaction 3.1:

$$\frac{1}{2}N_{2(g)} \leftrightarrow [N] \qquad (3.1)$$

where:

$N_{2(g)}$ refers to gaseous nitrogen (in steelmaking, this could be from the furnace atmosphere/atmosphere above the ladle – i.e. air, etc.) and [N] refers to nitrogen which is dissolved into the iron. Sieverts' law quantifies the equilibrium solubility of nitrogen:

$$ppm\ [N] = K_1\sqrt{P_{N_2}} \qquad (3.2)$$

where:

ppm [N] refers to the equilibrium amount (in parts per million) of nitrogen dissolved in iron at constant temperature;
K_1 is the equilibrium constant for equation 3.1;
P_{N_2} is the partial pressure of nitrogen gas in the relevant atmosphere (atm).

The relationship between the nitrogen partial pressure and the equilibrium amount of nitrogen that dissolves in iron, clearly indicates the importance of controlling the atmosphere to which liquid steel is exposed – higher partial pressures of nitrogen results in higher amounts of nitrogen dissolving in iron/steel. This has various implications in practice, as discussed in Chapter 4. Temperature and the structure of the iron matrix affect the solubility of nitrogen in iron, as shown in Figure 3.1.

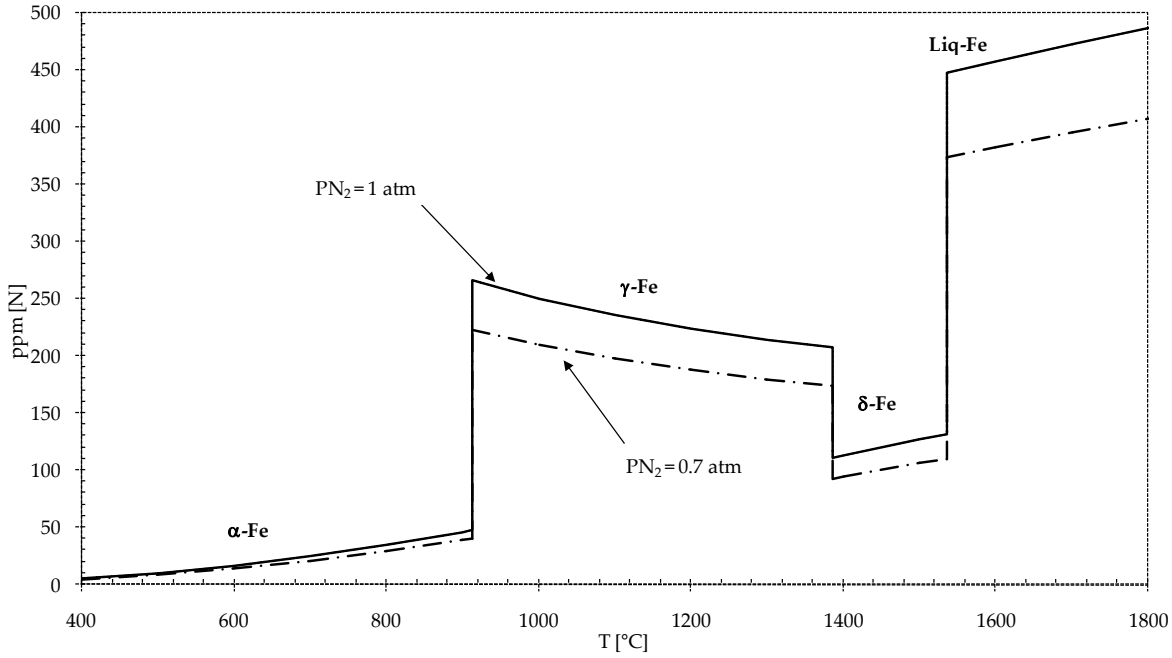

Figure 3.1: Solubility of Nitrogen in iron (calculated from data from the Steelmaking Data Sourcebook)[63]. A higher partial pressure of nitrogen above a steel melt increases the solubility thereof, as does an increase in temperature (in the case of nitrogen dissolution into liquid iron).

Although temperature has an effect on nitrogen solubility in *liquid* iron, the effect is slight (compared to the effect of partial pressure) when typical steelmaking temperatures (1600 – 1650°C) are considered.

The composition of the liquid steel also influences the solubility of nitrogen. A full analysis of this effect is beyond the scope of this project. Of primary importance is the interaction of nitrogen with elements such as carbon, aluminium, manganese, silicon, oxygen, niobium, chromium and titanium. Many of these elements form nitrides or carbo-nitrides (as explained in Chapter 2), whilst others enhance the solubility of nitrogen in liquid steel. The effect of composition on nitrogen solubility is quantified, thermodynamically, by the interaction coefficients of nitrogen with other elements in the melt. These interaction coefficients, in turn define the activity coefficient of nitrogen in liquid steel, which determines the amount of nitrogen that dissolves.

The amount of nitrogen which will dissolve into liquid steel is quantified by equation 3.3[10]:

$$h_N = f_N[\%N] \tag{3.3}$$

where: h_N is the Henrian activity of nitrogen in steel;
$[\%N]$ is the weight percent nitrogen dissolved into the liquid steel;
f_N is the activity coefficient, which is defined by equation (3.4):

$$\log f_N = \sum_{j=2}^{n} e_N^j (\%j) + \sum_{j=2}^{n} r_N^j (\%j)^2 + \sum_{j=2}^{n} \sum_{k=2}^{n} r_N^{j.k} (\%j)(\%k) + 0.(\%^3) \tag{3.4}$$

where: $j < k$
e_N^j is the first order interaction coefficient of N with element j;
r_N^j is the second order interaction coefficient of N with element j

The last two terms in equation 3.4 refer to higher order interactions, for which data is not available in steelmaking. Data for the first and second order interaction coefficients can be found in the text by Sigworth & Elliott[10] as well as a recent review article by for example, Siwka[11].

3.2. Kinetics of nitrogen dissolution into liquid steel

The dissolution and especially desorption of nitrogen into and from liquid steel have been found to be under kinetic control by various authors and have been reviewed in many steelmaking publications[e.g.12,14].

Oeters[12] and Turkdogan [13] are two of the many authors who reviewed the fundamentals of nitrogen mass transfer across a gas/iron interface. The general model is described below and is based on the texts of Oeters[12], Turkdogan[13] and Fruehan[14].

Nitrogen dissolution into liquid steel involves three consecutive steps, each of which can be rate determining:

1. *Transport of nitrogen in the gaseous phase to the gas/steel interface*

In the case of EAF steelmaking, where the furnace atmosphere contains a substantial amount of nitrogen this should not be rate limiting.

Fundamentally, the molar flux, $j_{N_2(gas\ phase)}$, of nitrogen is given by equation 3.5 as described by Oeters[12]:

$$j_{N_2(gas\ phase)} = -\frac{\beta_{N_2}}{RT}\left(P_{N_{2,interface}} - P_{N_{2,gas\ phase}}\right) \quad (3.5)$$

where: β_{N_2} is the mass transfer coefficient of nitrogen in the gas phase;
$P_{N_{2,interface}}$ and $P_{N_{2,gas\ phase}}$ is the partial pressure of nitrogen gas at the;
gas/steel interface and in the bulk gas phase respectively (atm);
R = 3.184 J.K^{-1}.mol^{-1} and T = Temperature (K)

A large difference in the partial pressure of gas in the furnace atmosphere and at the gas/steel interface would imply a large resistance to mass transfer, since nitrogen would have to diffuse through the gas phase towards the interface. When the partial pressures are equal, there is no significant resistance to gas mass transfer and this step is not rate limiting. When liquid steel is exposed to the atmosphere (initial stages of melting in an arc furnace, tapping, ladle transfers, etc.), the partial pressure of nitrogen is high (air contains 78% N_2), which implies that this step should not be rate limiting under normal steelmaking conditions.

2. *The chemical reaction (i.e. dissolution of N_2 into steel as dissolved N)*

The accepted[12,13,15,16] rate determining step for nitrogen dissolution into liquid steel has been found to be the rate at which nitrogen dissociates into adsorbed nitrogen onto the liquid steel surface, according to reaction 3.6:

$$N_{2(g)} \leftrightarrow N_2^{ads} \leftrightarrow 2[N] \quad (3.6)$$

The rate at which the dissociation of nitrogen (or rate of nitriding of liquid steel) occurs has been found to follow first order kinetics with respect to the nitrogen pressure, and is quantified by equation 3.7[13]:

$$\frac{d[\%N]}{dt} = \frac{100A}{\rho V} k_f (1-\theta)\{P_{N_2} - P_{N_{2,equilib}}\} \qquad (3.7)$$

where: ρ is the density of liquid steel

A the surface area of the melt which is exposed to nitrogen;

V is the volume of the melt;

$P_{N_{2,equilib}}$ is the equilibrium partial pressure of nitrogen at reaction time t, given by the equilibrium constant, K for nitrogen solubility $P_{N_{2,equilib}} = \frac{[\%N]^2}{K}$

In equation 3.7, k_f is the kinetic rate constant as determined by Byrne and Belton[15]:

$$k_f = 10^{\frac{-6340\pm(710)}{T}+1.85\pm(0.38)} \quad [\text{gN.cm}^{-2}.\text{min}^{-1}.\text{atm}^{-1}\ N_2] \qquad (3.8)$$

and 1-θ is the fraction of vacant sites on which nitrogen can be chemisorbed, as determined by various authors[15,16] quoted by Turkdogan[13]:

$$1-\theta = \frac{1}{1+260(\%O+\frac{\%S}{2})} \qquad (3.9)$$

Equation 3.9 and Figure 3.2 illustrate that oxygen and sulphur dissolved in liquid steel retard the rate at which nitrogen is dissolved into liquid steel, since these elements take up vacant sites on which nitrogen could have chemisorbed[14]. In practice, this has proven to be a valuable tool to avoid nitrogen pick-up by altering tapping and de-oxidation practice on an EAF steelmaking plant.

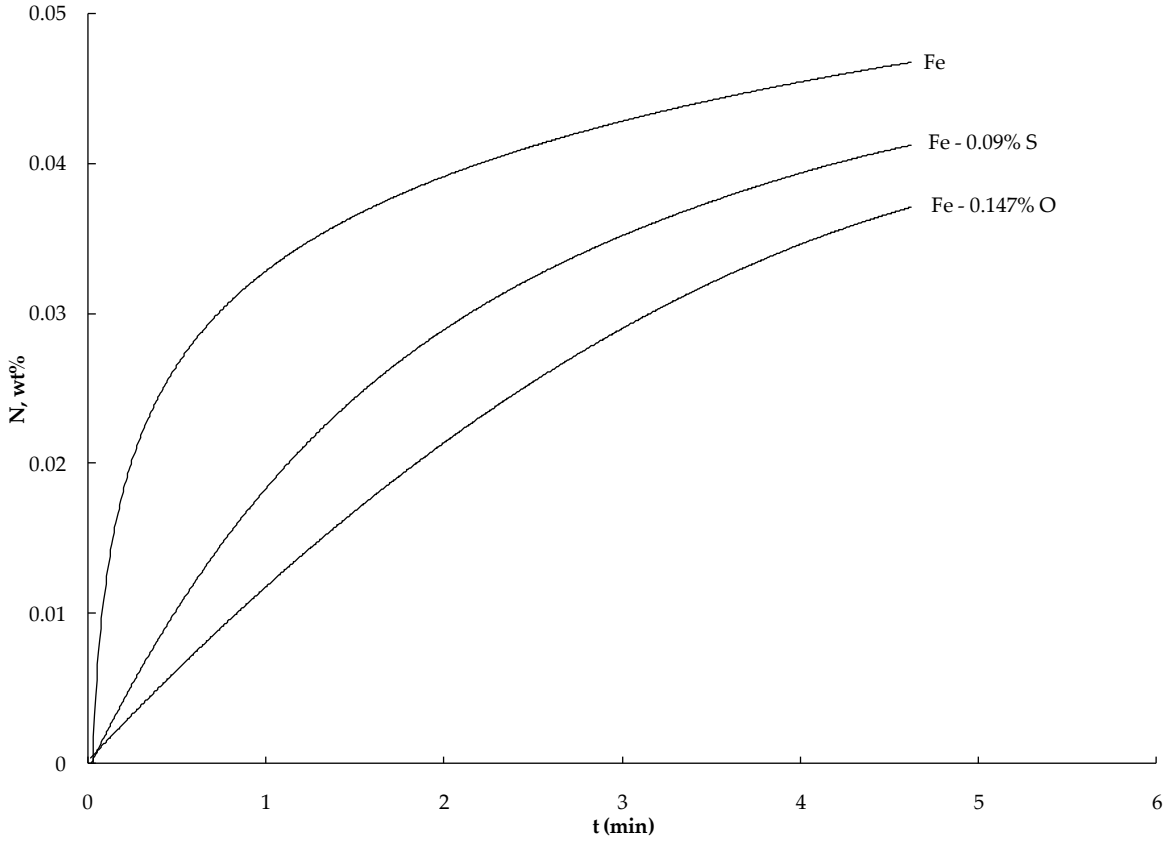

Figure 3.2: Effect of oxygen and sulphur on the rate of nitrogen absorption into liquid iron (redrawn from reference 14, p 17)

Essential to the above argument, is the fact that this project deals with steelmaking in an electric arc furnace – the dissociation and subsequent adsorption of nitrogen in a plasma environment (created by the arc) can be significantly faster, as outlined by more than one author – two references are of note in this regard. Katz and King[17] studied the kinetics of nitrogen absorption (and desorption) from a plasma arc into molten iron, in a refractory lined furnace (10 kg capacity) using a plasma torch. This is one of very few known *controlled* large scale experiments where iron was exposed to a nitrogen-argon plasma stream in the presence of surface active elements (in this case sulphur and oxygen), to establish the effect of the plasma arc melting on the dissolved nitrogen content. Mundra and Debroy[18] later reviewed the work of various authors to establish a general model for partitioning of gases between a metal and its plasma environment and applied their model to the work of, amongst others, Katz and King.

The general accepted model, based on the aforementioned work, for the enhanced solubility (i.e. higher than the thermodynamic equilibrium amount predicted by Sieverts' law) of nitrogen in molten iron due to the dissociation thereof in an arc, is as follows:

Diatomic nitrogen (in this case from the atmosphere in an electric arc furnace, to which the steel surface is partially exposed, depending on the bath condition / slag foaming behaviour) dissociates within the arc. The extent of dissociation is controlled by the nature of the generated arc – i.e. the nature of the power source (in the EAF as an alternating current conducted via solid graphite electrodes), system geometry as well as the nature of the diatomic gas – all of these properties are variable as mentioned by Mundra and Debroy[18], yielding a quite complex system, leading to difficulty in predicting the extent of dissociation for, for example, an arc furnace. This is also beyond the scope of this project. What is important is the fact that diatomic nitrogen dissociates at steelmaking temperatures according to the authors[18], resulting in the presence of monatomic nitrogen in the plasma arc.

The monatomic nitrogen (N) now readily absorbs on the metal surface from the metal-plasma interface, depending on the number of available surface sites (i.e. sites not occupied by mostly O and S – as discussed earlier). The faster adsorption (and enhanced solubility) was attributed to a higher than equilibrium (super-equilibrium) concentration of the atomic species near the metal surface. The calculations were done on the basis of the effective dissociation temperature, which was found to be approx. 100-300K above the surface temperature of the metal.

Figure 3.3 is a schematic diagram illustrating the concept of plasma. In the case of EAF steelmaking, G_2 would be N_2, with the remainder of the gas mixture consisting of $CO/CO_2/H_2O_{(g)}/H_2$ and other smaller amounts of gaseous species.

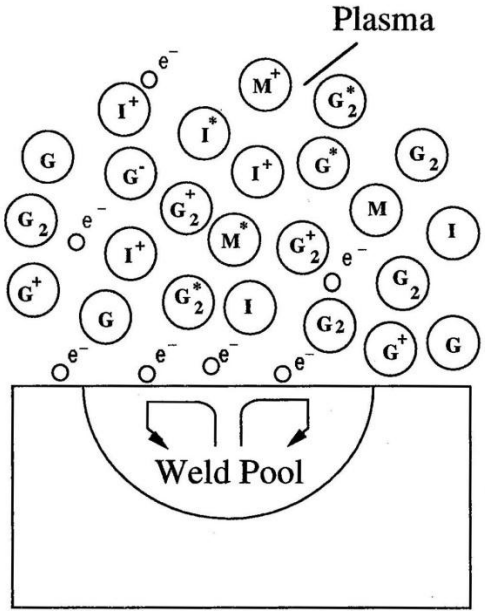

Figure 3.3: Schematic diagram of gaseous species near a metal exposed to plasma. Plasma consists of electrons (e^-), neutral atoms (G,I,M) and molecules (G_2), excited atoms (I*,G*,M*) and molecules (G_2*), and ions (G^-,G^+,G_2^+,I^+), where G=gas, M=metal, and I=inert gas[18].

Although the solubility of nitrogen is enhanced by the arc, gas bubbles will tend to form when the thermodynamic solubility limit of nitrogen is reached.

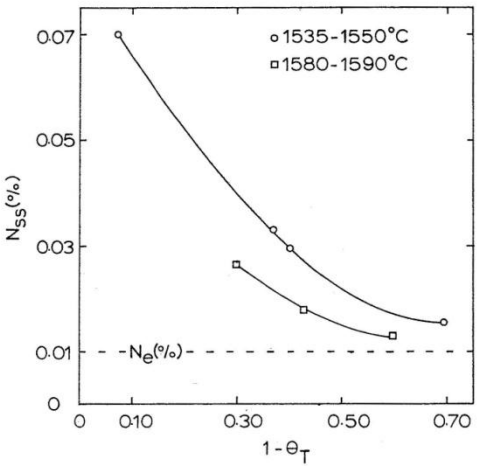

Figure 3.4a: Steady state (i.e. the nitrogen content where the rates of adsorption and desorption of nitrogen into and from iron is equal) nitrogen content of iron as a function of surface availability. N_e (%) refers to the equilibrium nitrogen content[17].

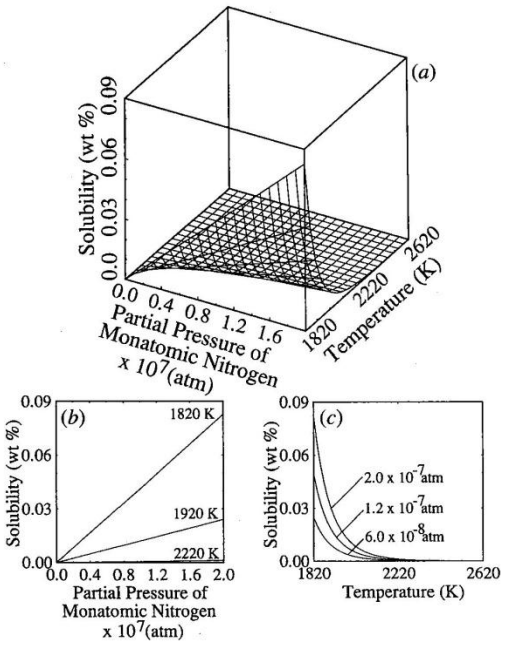

Figure 3.4b: From the calculations of Mundra and Debroy[18]: Equilibrium solubility of nitrogen in iron exposed to monatomic nitrogen as a function of temperature and partial pressure of monatomic nitrogen. The figures are included to substantiate the claim of enhanced solubility of monatomic nitrogen in iron.

3. *Nitrogen transport within the melt*

If none of the above two steps are rate limiting, the only remaining step which could be rate limiting is nitrogen transfer from the interface of the melt into the melt itself. A description of this is available in the text by Oeters[12]. The nature of a steelmaking melt is such that there is usually a sufficient degree of mixing/bath movement, to allow for rapid mass transfer of nitrogen from the interface into the melt. Oeters[12] concludes that this step is not rate limiting under steelmaking conditions.

In conclusion – the rate of nitriding of liquid steel, a first order kinetic process with respect to nitrogen pressure, is determined by the rate at which nitrogen dissociates at the gas/steel interface and is retarded by the presence of oxygen and sulphur. Furthermore, the absorption of nitrogen into steel in the EAF can be substantially faster due to the dissociation of diatomic nitrogen to the monatomic state.

3.3. Kinetics of the removal of nitrogen from liquid steel

The removal of nitrogen from liquid steel *after* steelmaking is addressed first, as the removal of nitrogen *during* steelmaking is addressed in Chapter 4.

For chemical control, the rate of removal of nitrogen is second order with respect to the concentration of dissolved nitrogen[13,19]; the reaction is shown below:

$$2[N] \leftrightarrow N_{2(g)} \tag{3.10}$$

The rate at which nitrogen can be removed is quantified by equation 3.11:

$$\frac{1}{\%N} - \frac{1}{\%N_0} = \frac{100A}{\rho V} k_r (1-\theta) t \tag{3.11}$$

where: ρ, A, V, t and $(1-\theta)$ refer to the same constants/variables as in equation 3.7

In equation 3.11, however, k_r is the rate constant for the reverse of reaction 3.6, or then the rate constant for the rate at which nitrogen recombines to form nitrogen gas (reaction 3.8) and is given by:

$$k_r = 10^{\frac{-5964}{T}+4.33} \qquad [\text{gNcm}^{-2}.\text{min}^{-1}.\%\text{N}^{-1}] \tag{3.12}$$

Equation 3.12 is deduced from $k_r = k_f/K$, where K is the equilibrium constant for nitrogen dissolving into liquid iron[13]:

$$K = \frac{[\%N]^2}{P_{N_2,equilib}} = 10^{\frac{-376}{T}-2.48} \tag{3.13}$$

3.3.1. Nitrogen removal by gas bubbling after steelmaking

Inspection of reaction 3.10 reveals that nitrogen removal should be simple, at least from a thermodynamic point of view – a lower partial pressure (achieved by either gas bubbling or by reducing the total pressure of the process by drawing a vacuum within the vessel) of nitrogen gas, should decrease the nitrogen content of steel, yet this is not practicable, due to the kinetic nature of the nitrogen removal process. This has been reported in literature[13,14,] several times and is briefly discussed here.

Bubbling of an inert gas, e.g. argon through a steel melt lowers the partial pressure of nitrogen, facilitating nitrogen removal. The removal of nitrogen by gas bubbling is considered to be under mass transfer (gas/bubble reactions) and chemical reaction control, in series, as stated in various texts[13]. It has been shown, by example calculations[13], that high volumetric flow rates of gas eliminate mass transfer as a rate limiting step and that the rate of nitrogen removal is then principally under chemical reaction control, with dissolved oxygen and sulphur playing a significant role in nitrogen removal. Oxygen and sulphur block adsorption sites on bubbles where the nitrogen could have recombined to form molecular N_2.

The maximum rate at which nitrogen can be purged from a steel melt (provided that the rates of the diffusion processes and chemical reactions are high enough and that argon bubbles moving through the melt will saturate themselves with nitrogen) is described by equation 3.14[13]:

$$\frac{1}{ppm\ N} - \frac{1}{ppm\ N_0} = \frac{M\dot{V}}{22.414x10^{-3}K^2\bar{P}}t \qquad (3.14)$$

where: ppm N is the nitrogen content at time t in ppm
ppm N_0 is the initial nitrogen content in ppm
M is the molecular mass of the diatomic gas being purged (nitrogen)
$\dot{V}$ is the volumetric flow rate of argon in $Nm^3.min^{-1}.t^{-1}$
K is the equilibrium constant at the relevant temperature
$\bar{P}$ is the average bubble pressure in the melt (atmospheric plus ferrostatic)

For a temperature of 1650 °C and an average bubble pressure of 1.5 atm, equation 3.14 reduces to:

$$\frac{1}{ppm\ N} - \frac{1}{ppm\ N_0} = 0.00395t \qquad (3.15)$$

For hydrogen removal, the equivalent maximum rate is given by equation 3.16:

$$\frac{1}{ppm\ H} - \frac{1}{ppm\ H_0} = 0.0804t \qquad (3.16)$$

From the equations above, it is clear that the maximum rate of nitrogen removal is much lower than that for hydrogen.

Assuming a volumetric flow rate of 2 $Nm^3.min^{-1}.t^{-1}$ of argon, for 2 minutes[13], an initial amount of 60 ppm N would only be reduced to 54 ppm, whilst for hydrogen, two minutes of purging would reduce an already low 7 ppm H to 2 ppm.

The above implies that after steelmaking, large volumes of inert gas along with a substantial amount of time, is essentially not worth wasting in an attempt to denitrogenate a steel melt, due to unfavourable kinetics.

3.3.2. Nitrogen removal by vacuum degassing

By lowering the total pressure above a steel melt, the nitrogen removal reaction should be driven forward, based on the application of Le Chatelier's principle to reaction 3.10. Bannenberg et al[20] developed a mixed control model to quantify the removal of nitrogen in a tank degasser. Trials on an industrial scale and calculations based on a model developed from test data showed that only some nitrogen is removed (again, the rate is low), and then only if the steel is fully de-oxidised with a low concentration of sulphur. The rate of nitrogen removal under vacuum is controlled by liquid phase mass transfer at low O and S contents, whist it is under mixed or chemical reaction control for higher O and S contents (for the same reason as stated in the previous section)[14,20]. The rate equation (slightly adjusted version of equation 3.11 as done by Turkdogan[13]), is given below:

$$\frac{1}{ppm\ N} - \frac{1}{ppm\ N_0} = k_N(1-\theta)t \qquad (3.17)$$

where k_N is the apparent rate constant for nitrogen removal at low values of O and S, i.e. as these approach zero. The constant has a value of 0.0013 (ppm N.min)$^{-1}$ for 180 t heats at 1 mbar tank pressure with an argon flow rate of 1.8 Nm^{-3}.min^{-1}. Turkdogan[13] also mentions that this value is decreased greatly with a decrease in argon bubbling rate, due to liquid phase mass transfer which would then become rate limiting.

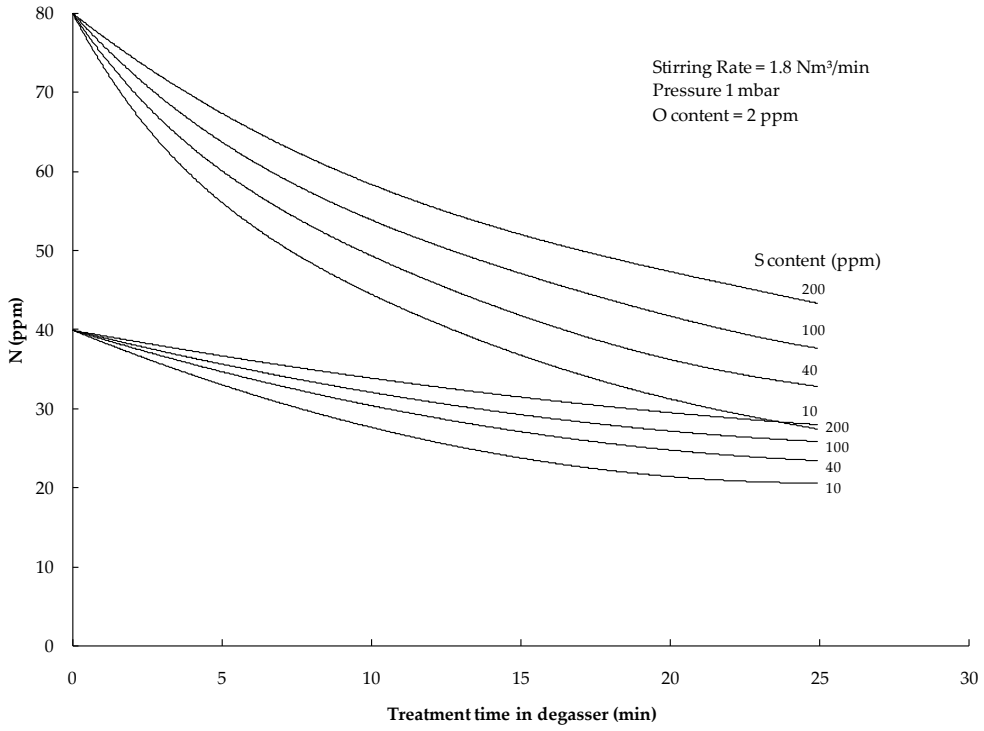

Figure 3.5: Calculated effect of sulphur on denitrogenisation in tank degasser with argon stirring rate of 1.8 Nm³/min, redrawn from reference 13, p 284.

Figure 3.5 emphasises both the effect of dissolved sulphur (i.e. higher sulphur contents retard nitrogen removal), as well as the effect of treatment time (longer treatment times do not necessarily yield significantly lower final nitrogen contents) and the initial nitrogen content (lower initial nitrogen content causes a lower removal rate, as is expected).

In the article by Bannenberg et al[20], the effect of the volume of stirring gas is also illustrated; this is shown in Figure 3.6. High inert gas volumes, low initial nitrogen contents, and low dissolved sulphur and oxygen contents result in the lowest possible nitrogen content after a degassing treatment. Figure 3.7 shows that increased amounts of stirring, in desulphurised steels, reduces the amount of nitrogen (i.e. mass transfer control dominates, as the chemical reaction is not impaired by O or S). On the specific plant, from which this project originated, the vacuum arc degasser, is said[21] to aim to reduce the nitrogen content of 150 tons of liquid steel from approx. 80 to 45-55 ppm within 20 minutes at a target final vacuum of 10mbar (there was insufficient data supplied from the plant on this unit to support this statement). At this plant, the heating rate which the VAD can achieve is extremely low (~1 °C/min), vs. the two ladle furnaces which can achieve ~4-5 °C/min), resulting in additional heating time required before continuous casting. This remains an extra processing step, which should, as in any efficient process, be avoided.

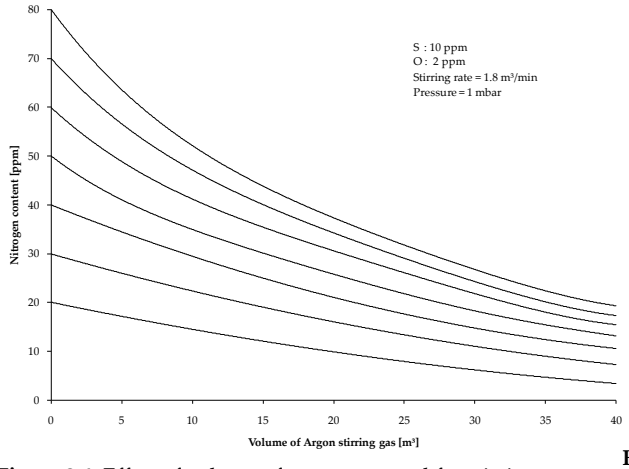

Figure 3.6: Effect of volume of argon gas used for stirring a ladle on the final nitrogen content of liquid steel after vacuum degassing (redrawn from reference 20). The lines are drawn for different initial nitrogen concentrations (i.e. at volume of stirring gas = 0 m³, the initial nitrogen value is the y-intercept)

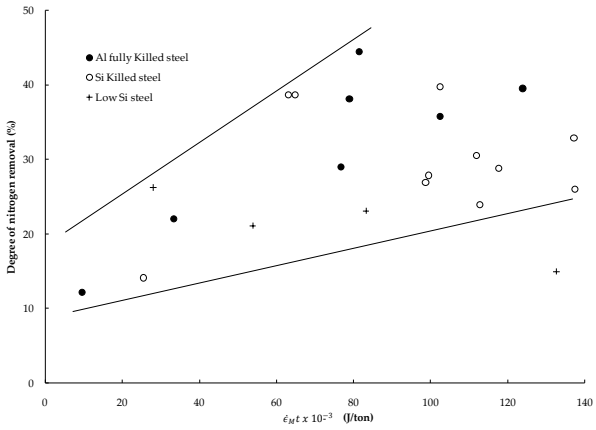

Figure 3.7: Effect of stirring rate on the degree of nitrogen removal from a desulphurised steel during vacuum treatment, redrawn from reference 14, p 42, original reference is Suzuki et al[22]

In conclusion - Thermodynamically, approximately 406 ppm nitrogen can dissolve into liquid iron, if exposed to air at 1600 °C. However, the dissolution of nitrogen into liquid steel is not an equilibrium process and is kinetically controlled. The rate limiting step for dissolution under electric steelmaking conditions is the dissociation of diatomic nitrogen gas and subsequent chemisorption thereof onto the liquid steel surface, the rate of which is retarded by the presence of surface active elements (especially dissolved oxygen and sulphur), due to the reduced number of surface sites on which chemisorption can occur. The removal of nitrogen from liquid steel is hence also kinetically limited. Strategies to remove nitrogen include bubbling of an inert gas (e.g. argon) through the steel melt, in a ladle or within a degassing unit. The rate of removal by bubbling is limited by mass transfer and/or chemical kinetics, but the rate of removal is much lower than for, for example, hydrogen - making removal of nitrogen by inert gas bubbling impractical for a typical meltshop. Vacuum degassing can also reduce the nitrogen content, provided the steel is low in sulphur and oxygen and high volumes of stirring gas is used. Use of a vacuum degasser for each heat would also result in a decrease of the production rate of a steel plant, in addition to adding cost to the process. In the next chapter, alternative methods of nitrogen removal are discussed as well as strategies to limit the amount of nitrogen taken up by liquid steel in the first place.

3.4. Nitrogen Control in Electric Steelmaking

Nitrogen control in EAF steelmaking can be successfully achieved by applying three principles[23]: using feed materials with low nitrogen levels; preventing absorption of nitrogen from the atmosphere and by removing nitrogen during or after steelmaking. Trotter et al[23] proposed a schematic of these approaches, redrawn here as Figure 3.8.

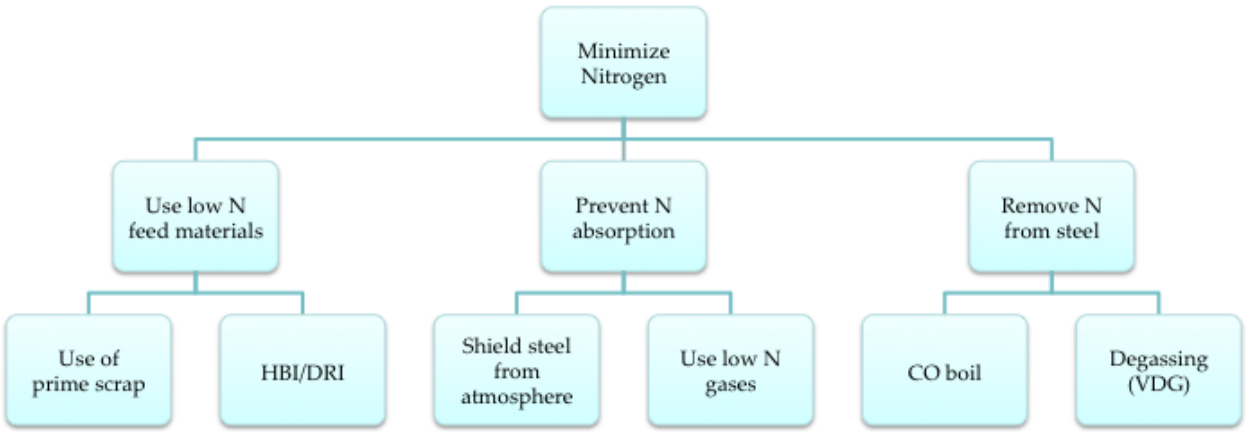

Figure 3.8: Strategies for minimising nitrogen levels in an EAF[23].

In this section, the topics are discussed in a similar fashion, but more emphasis is placed on the role of DRI.

3.4.1. Foaming slag practice as a tool to prevent nitrogen adsorption by steel

The slag layer expands as bubbles of CO (and other gases) move through the slag, forming a "foaming slag".

The formation of a foaming slag during EAF steelmaking is beneficial, since this "foam" protects the steel against the atmosphere, limiting nitrogen pickup; it also improves energy efficiency. This is a well-known phenomenon for steelmakers alike – both in EAF and BOF steelmaking.

Aside from shielding the steel melt from the atmosphere, many other benefits have been reported when a foamy slag forms, which include reduced refractory wear, less heat radiated to the side walls and roof of the furnace, enhanced energy efficiency (and less heat loss), less power-on time, less dust, reduced flicker, improved arc stability, etc.

Slag foaming has been studied in depth by many authors and the "success" of a foaming slag is quantified largely by a "foaming index" - this index measures the average time it takes for a gas bubble to flow through the foam formed. Many models exist to calculate this index[24,25], which essentially is a ratio between slag properties, i.e. slag viscosity, density and surface tension (which is a function of slag chemistry) as well as the average bubble diameter of bubbles within the foam. In general, the foaming index is inversely proportional to bubble diameter (with varying exponents). To this end, more stable foams are generated (provided the slag chemistry is correct) when finer bubbles are formed in the slag phase.

To foam a steelmaking slag effectively, the composition thereof should be correct – one of the first studies done by Ito & Fruehan[26,27] showed this effect – ultimately, the viscosity of the slag should be high, with a low surface tension. Optimal slag chemistry for the most stable foams been reported[28,29,30,31]. Slag foam stability varies during the melting time, hence slag formers are already added to the basket to achieve a slag quickly and to ensure that this slags foams early on. Optimal slag foaming was found by Ito and Fruehan[26] at 20% FeO, with a CaO/SiO_2 of 1 at 1600 °C in a $CaO\text{-}SiO_2\text{-}FeO$ slag. It should be noted that FeO affects the viscosity of the slag substantially, also shown by the authors mentioned.

Another essential component of the foaming slag is the bubbles. As stated earlier in this section, the diameter of bubbles formed is critical for foam stability. In addition, smaller bubbles in steel (of gasses like CO and Ar), are active sites for removal of nitrogen: increased amounts of smaller/finer CO bubbles would increase the amount of surface area for nitrogen removal, flushing out more nitrogen from the melt.

The formation of CO bubbles (by supersaturation of the metal droplet with CO, overcoming the surface tension of the molten steel surface) within a steel melt, occurs when dissolved carbon reacts with dissolved oxygen:

$$\underline{C} + \underline{O} = CO_{(g)} \qquad (3.18)$$

This is commonly referred to "CO boil" or "Carbon Boil" in steelmaking. The higher the degree of carbon boil that can be achieved, the more nitrogen can be flushed from the melt.

The phenomenon was explained by Sun et al[32,33] and is influenced by temperature, as well as sulphur content of the melt. Since the reaction to produce CO bubbles is an interfacial one between dissolved species, transport of dissolved carbon and/or oxygen or the interfacial reaction can be rate controlling, along with CO transport away from the interface. Sun[32,33] found that the rate controlling step was carbon transport. In EAF steelmaking, carbon is injected with oxygen to bring about carbon boil, with typical melt-in carbon contents of 0.2-0.3%C at the plant studied in this project.

Injection of carbon (the particular plant in question uses anthracite as carbon source) and oxygen is only one way to produce CO bubbles. Alternative studies[34,35], using iron carbide as injectant have been carried out with varying success. The economics of using iron carbide as injectant is usually unfavourable to start with, along with some technical issues worth mentioning:

Firstly, the grade of iron carbide needs to be quite high (iron carbide products of low grade, have been postulated to react at lower temperatures, e.g. as low as 700 ˚C, potentially blocking an injection lance[34]);

Secondly, injection of iron carbide is not as an attractive option as charging the material into a basket – where the close proximity of the carbon source to the melt enhances the overall efficiency of using the carbide – to aid slag foaming behaviour, the injectant might be more effective;

Thirdly, the use of iron carbide, involves using a significant amount (up to 30% of the basket charge) thereof[35] (when compared to high carbon HBI, this might not be cost effective).

Lastly, the supply of iron carbide could be a problem. The work reported by Ruer[35] in 1996, showed improvements, but the plant producing iron carbide is no longer operational – this is just one example.

Many operating plants do carbon adjustments by injection of carbon (in this case anthracite of which the consumption is between 20-60 kg/ton of tapped steel, which is cheap in comparison to iron carbide) and oxygen to sustain a foaming slag, along

with ensuring the final carbon content of the tapped steel to be correct. To this end, this is still the most viable option to sustain foaming slags, along with ensuring that the slag chemistry is correct. The rule of "take care of the slag and the metal will take care of itself" still applies, even in this context – the correct slag chemistry brings about a foaming slag, which in turn protects the steel melt from taking up nitrogen from the atmosphere, with additional benefits as mentioned.

Many authors have investigated the benefits of having sufficient amounts of carbon in DRI to reduce nitrogen levels in liquid steel during electric steelmaking[36,13,39]. Carbon, when present in sufficient levels (approx. 1.8%), yielded substantial improvements in slag foaming properties[39] by the promotion of carbon boil. In addition, trials have also been run on injection of fine DRI material into steel melts to essentially start the carbon boil within the steel melt[37]. There needs to be a balance between the amounts of carbon and oxygen present in DRI (1% C balances around 6% FeO, yielding CO and metallic iron when heated), to promote slag foaming and hence shielding the bath from the atmosphere.

Goldstein and Fruehan[55] showed that when DRI is dropped into a metal-slag melt, that DRI does not necessarily penetrate the metal, but rather "floats" on top of the melt (at the slag/metal interface), releasing carbon as carbon monoxide gas, foaming the slag, but not increasing the carbon content of the melt. This implies that the use of DRI to increase the carbon content of a steel melt is limited (if at all possible), yet various plants appear to benefit from using DRI with higher carbon content than that produced via the rotary kiln route.

3.4.2. The Use of Low Nitrogen Feed Materials

Use of Prime Scrap

Prime scrap, which has low levels of residual elements, low nitrogen levels and is relatively un-oxidised, is an ideal feed material to an EAF. The problem is that this type of scrap is either not available or more expensive than other types of scrap, e.g. scrap originating from the plant itself, scrap purchased from scrap dealers, etc. More often than not, not much is known of the chemistry of scrap charged. EAF plant engineers often use combinations of prime, purchase and revert scrap and evaluate the overall chemistry of the liquid steel to find an optimal combination which will fit the plant steelmaking cost model, which in turn limits the amount of direct control of nitrogen content in this way. The amount of nitrogen in scrap can vary – Trotter[23] quotes a figure of 30-120 ppm, but every piece of scrap cannot be analysed.

Use of DRI/HBI in EAF Steelmaking

A substantial amount of work has been dedicated to the numerous benefits as well as disadvantages of using DRI/HBI in EAF Steelmaking – this is well summarised by Scarnatti[38] and also Jones[39]:

a. *DRI/HBI contains very little tramp elements and is a relatively clean iron unit*
The implication is that DRI contains roughly 88-94% Fe and the rest is gangue material including residual FeO, and in the case of DRI produced via gaseous reduction processes, between 1 and 3% carbon. Higher gangue contents result in lower iron yields, increased flux- (to keep the slag basic) and power consumption (to melt the extra gangue and fluxes);

b. *DRI/HBI has a relatively uniform size distribution, which has various benefits*
Compared to scrap, the size of DRI is uniform, making melting and handling easier. In addition, the uniform, relatively small size (in this project, DRI is smaller than 25 mm on average) allows for continuous charging of the DRI through the roof of the furnace. In practice, the temperature of the steel melt is dynamically controlled by controlling the feed rate of DRI charged through the roof of the furnace. Smaller sized DRI (usually sub 3mm) is charged to the scrap bucket; otherwise this material would be sucked off by the furnace off-gas system.

c. *The use of more DRI/HBI increases power consumption*
Since unreacted FeO and gangue remain in DRI, between 100-200 kWh/t of additional electricity is required, when compared to scrap only processes. The benefits far outweigh the cost of this electricity. To this end, electric steelmakers opt for the maximum amount of metallisation when blending DRI, to avoid this extra cost – it is however not something that can be directly controlled by the *steelmaking* plant.

d. *Other benefits*
Other benefits includes less flicker, no need for scrap recharging, no need to open the roof during melting, less noise during meltdown, easy slag foam generation, more predictable price structure than scrap.

An exhaustive account of all the benefits of using DRI in EAF steelmaking is beyond the scope of this report, hence only a few highlights were given, as the plant considered here operates on DRI – the nature of the particular DRI used, is what is important, as this was found to influence the nitrogen content of the steel tapped.

The Nature of Direct Reduced Iron

Direct Reduced Iron (DRI) is produced via two main routes, when classified on the basis of the reductant (or process) used. Direct Reduction Plants where cheap coal is readily available and natural gas (or another source of cheap reducing gas) is not, produce DRI through a rotary kiln process, e.g. the ArcelorMittal plant in Vanderbijlpark (specifically where the SL/RN process is used), whilst the same company uses the MIDREX technology at Saldanha Bay, where COREX top gas and natural gas are available. Both processes reduce iron ore (different types are used) to produce a solid product, but the nature of the product produced differs substantially in terms of chemistry and final form.

Anameric and Kawatra[40] reviewed all of the different DRI processes well, along with the products that come from them. Again, classification can be done the basis of reactor type, reductant used, etc., but they present an important summary of the properties of DRI, as depicted in Table 3.1.

Table 3.1: Difference in nature of DRI processes and products as compiled by Anameric and Kawatra[40]

	Natural gas-based direct reduction processes	Coal-based direct reduction processes
Reactors utilized for reduction reactions	Vertical Shaft Furnace, retort (batch) furnace, fluidized bed reactor	Vertical shaft furnace, multiple hearth furnace, rotary kiln, rotary hearth furnace, fluidized bed reactor
Reducing–carburizing agent	Reformed natural gas	Non-coking coals, charcoal, coke breeze
Iron oxide feed stocks	Pellets, lump, and fine ore	Pellets, lump, and fine ore, green balls, iron oxide waste materials
Reduction Temperatures (°C)	850-950 °C	950-1050 °C
Operating Pressures (atm)	1-16 atm	Slightly positive
Product % Metallization	85-95%	88-92%
Ease of metallization control	Can be adjusted by reduction and cooling gas composition (Commercially practiced)	Hard to achieve
Product % carbon	1-2.5%	~0.2%
Ease of carburization control	Can be adjusted by reduction and cooling gas composition (Commercially practiced)	Hard to achieve

In conclusion: nitrogen pick-up in the EAF is inevitable, but can be controlled. To this end, careful control of the furnace raw material input and good operating practice (e.g. using a foaming slag, using DRI as feed, having sufficient amounts of carbon in the charge, etc.) can make a substantial difference. DRI produced via coal-based processes are inherently different to those produced via gas-based processes and hence the steel product will also be different, since the chemistry of DRI (i.e. %C, which aids in nitrogen removal) from the different processes differs.

Chapter 4:
DRI as a source of nitrogen in electric-furnace steelmaking

4.1. Hypotheses

Two main hypotheses were tested in this work:

1. Direct-reduced iron can cause nitrogen pick-up in electric-furnace steel-making.
2. Nitrogen pick-up can be effectively countered by ensuring a sufficiently high melt-in carbon content, even in the plant where nitrogen is picked up from direct-reduced iron.

These hypotheses were tested using the following approach:

1. The possibility that nitrogen can be picked up from direct-reduced iron was tested in three ways:
   a. Plant data on tap nitrogen contents were analyzed, to determine whether heats with higher proportions of direct-reduced iron (relative to scrap) had lower nitrogen levels. Lower nitrogen levels would be expected if the direct-reduced iron had low nitrogen, and diluted the nitrogen content of the scrap. (Results presented in this chapter.)
   b. Direct-reduced iron was analyzed chemically, to determine its nitrogen content. (Results presented in this chapter.)
   c. The feasibility that the direct-reduced iron can pick up nitrogen during reduction and subsequent cooling was assessed with simple kinetic models of the main steps that can lead to nitriding of SL/RN direct-reduced iron. (Results presented in Chapter 5.)
2. The effect of melt-in carbon was also tested by analyzing plant data, correlating tap nitrogen with melt-in carbon content. The observed relationship (of lower tap nitrogen if the melt-in carbon content was higher) was compared with the expected relationship if evolved carbon monoxide flushes nitrogen from the steel, and the carbon monoxide bubbles are saturated with nitrogen gas when leaving the steel. (Results presented in Chapter 6.)

4.2. Process description of the EAF plant (brief)

The electric steel plant produces crude steel (with roughly 0.03%C) using three electric arc furnaces (each 96MVA) mainly from scrap and DRI, tapped at approximately 1630 ˚C. Each furnace has a capacity of 180 tons, of which 155 tons is tapped, on average, from each heat. On average the charge make-up is 30% scrap,

50% DRI, and 10% hot metal (from a blast furnace), with the remaining 10% consisting of pool iron and high carbon residue. Direct-reduced iron is charged in the initial basket (together with scrap) and is also charged continuously through the furnace roof (later in the melting period); the ratio between the amount of DRI in the basket and the amount charged through the roof is typically 1:5. DRI that is smaller than 3 mm is charged in the scrap bucket (and constitutes around 8% of the metallic charge), whereas larger material (up to ~25 mm) is charged through the furnace roof (approximately 40% of the metallic charge is roof DRI).

At tap, the steel on average contains 800-1100 ppm dissolved oxygen. Following tapping, de-oxidation of the liquid steel is carried out with Al, Si or both, after which the ladle is sent to secondary metallurgy. The aim dissolved oxygen content is 10ppm on arrival at secondary metallurgy, to limit Al-wire consumption at the ladle furnaces. Desulphurization and alloy addition are carried out at one of three ladle stations. Hydrogen sensitive grades (typically with $\underline{H} \geq 7$ppm) are treated in a Vacuum Arc Degasser. The steel is subsequently cast into slabs, using a continuous caster.

The desired nitrogen content at tap is as low as possible; acceptable levels would generally be below 80 ppm.

A typical steelmaking heat comprises a few steps (schematically shown as figure 4.1a), and summarized below:

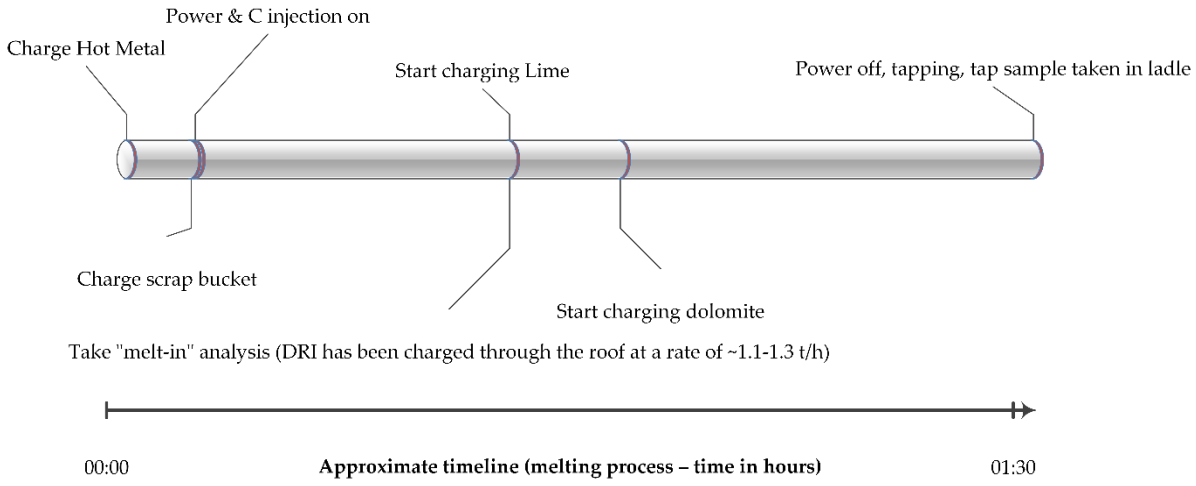

Figure 4.1a: Approximate timeline for smelting process in an EAF as considered in this project.

1. Hot metal (if used) is charged first into the 15-30 ton "hot heel" left behind after the last heat.
2. The first basket is charged. This basket contains scrap and DRI fines (size ≤ 3mm), together with some slag formers, coke fines, and pool iron.
3. The roof is swung closed and the power is switched on.

4. After arcing for roughly 45-60 minutes into the process, the first melt-in analysis is taken, while arcing continues. At this stage most of the scrap (some DRI would be charged by this time as well for ~20 minutes), is molten, but heavy scrap can still be only partially molten.
5. DRI, with additional fluxes, is subsequently charged continuously through the roof. Continuous charging (of DRI) lasts roughly 70 minutes at a rate of 1.1-1.3 t/min.
6. Another steel sample is taken, preferably after DRI feeding has stopped.
7. The operator starts blowing carbon and/or oxygen into the melt to aid the formation of a foaming slag by inducing "CO boil". This process continues until the steel is fully liquid and ready for tapping.
8. One last sample is taken, for analysis of the final carbon, nitrogen and oxygen levels. Carbon is to be adjusted to specification, nitrogen checked (if levels are elevated, the material might be re-classed) and the oxygen level is used to assess the amount of de-oxidant (Al, Si or both) to be added during tapping.
9. The furnace is tilted and tapping commences through an eccentric bottom taphole at the back of the furnace. The aim tapping time is less than 3 minutes (on average 2.5 minutes is achieved), to limit slag carryover and nitrogen pickup.

4.3. SL/RN direct-reduced iron process description and the possible effect of nitrogen in DRI contributing to the liquid steel nitrogen content

As background to tests of the effect of SL/RN direct-reduced iron on nitrogen pick-up, the main features of the SL/RN are briefly summarized here.

The SL/RN rotary kilns & cooler on the plant in question

Coal-based DRI processes (such as SL/RN) only make up a small portion of the world DRI production, but remain significant in South Africa (and also in India), due to the availability of cheap coal, suitable ore and the fact that natural gas is not readily available inland where the plant is situated. Approximately 1.5 tons of ore, 800 kg of coal and 40 kg of dolomite are fed to a rotary kiln (a typical kiln at Vanderbijlpark is 80 m in length, with an internal diameter of 4.8 m) to produce 1 ton of DRI. The average residence time in the reduction kiln is approximately 12 hours. The DRI produced in the kiln exits at approximately 1000°C (the temperature in the transfer chute which connects the kiln and cooler is in the range of 1050-1150°C). A schematic (not to scale) of the process is shown in Figure 4.1b.

At the kiln exit, the material passes through a transfer chute (closed off from the atmosphere), dropping into a rotary cooler. The cooler is 50 m long and has an internal diameter of 3.6 m.

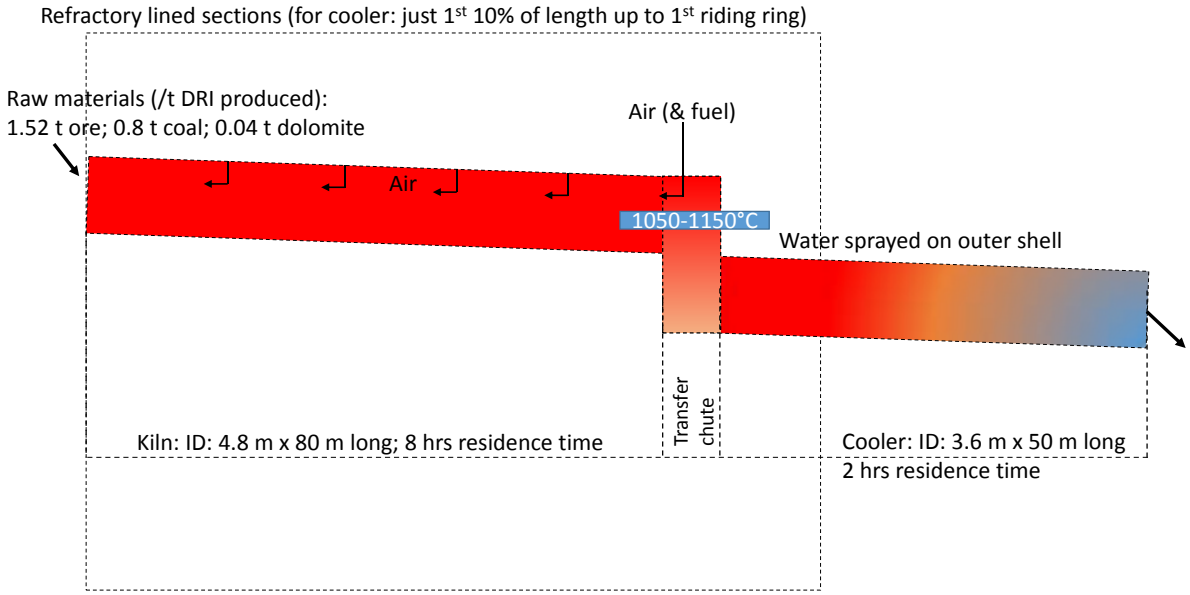

Figure 4.1b: Schematic of the SL/RN process (essential elements only, not to scale)

During the residence time of approximately 2 hours in the cooler, the material cools to approximately 100°C. The reduction kiln is refractory lined (mostly with alumina castables), whilst the cooler is only lined with refractories up to the first riding ring (situated approximately 5 meters from the centerline of the transfer chute). The rest of the length of the cooler is fitted with lifter bars to allow for material to be transferred through the air to enhance cooling. Cooling is achieved by spraying water onto the steel shell of the cooler (the shell, in turn, is in contact with DRI). The reduction kiln atmosphere consists mainly of nitrogen, carbon dioxide and water vapor; the atmosphere in the cooler is expected to be mainly nitrogen and carbon dioxide.

Since the process is a solid-state reduction process, with solid carbon as reductant, virtually no carbon dissolves in the sponge iron. Carbon values for DRI produced at this plant is less than 0.15% C[41], considerably lower than that of DRI produced by gaseous reduction processes (such as MIDREX), for which the carbon content of the DRI ranges between 1 and 2.5%[40]. For gas-based processes, the DRI is carburized by cooling in a methane/hydrogen mixture (after reduction). In the rotary kiln, virtually no carbon is picked up, since most of the atmosphere is non-carburising. Although a figure of 0.2% C is quoted in Table 3.1, the carbon content of the SL/RN product at the plant studied here is never above 0.2%, similar to the value of 0.07% carbon quoted in the original article on the SL process[42].

The details of the SL/RN process are expected to be significant to nitrogen pick-up during subsequent electrical steelmaking, for two main reasons. First, the low carbon content of the SL/RN DRI does not contribute to melt-in carbon or to slag foaming and hence does not promote nitrogen removal during steelmaking. Second,

the SL/RN DRI may pick up nitrogen from the furnace and cooler atmosphere during the later stages of reduction or during cooling; nitrided SL/RN DRI would increase the nitrogen content of the steel melt.

4.4. Nitrogen in DRI: Effect on tap nitrogen content of EAF steel

Plant data analysis: approach

Plant data were analyzed to test whether SL/RN DRI contributes to nitrogen pick-up. Data for steel production on all three electrical furnaces for June 2006 were analyzed. A total of 682 heats had complete metal analyses for nitrogen.

In this analysis, data for heats where hot metal was used were excluded, as the amount of hot metal is variable and it is a carbon source, which would diminish nitrogen pick-up. The main variable between different heats was hence the proportion of direct-reduced iron in the charge.

A second factor which affects tap nitrogen is the extent to which slag foaming is maintained. The plant operates a system which monitors the "foaminess" of the slag electronically, yielding an index. Heats with an index greater than 50% are regarded as having well-foamed slag; results were hence filtered to only include heats with well-foamed slag.

After applying these two filters – excluding both heats with hot metal in the charge and ones with poor slag foaming – a total of 270 heats remained.

Plant data analysis: results

The relationship between tap nitrogen content and the proportion of DRI in the charge (for the 270 heats) is summarized in Figure 4.2. From Figure 4.2, it can be seen that, for this plant, more DRI charged to the furnace (as a percentage of the total metal charge) did not result in a lower tap nitrogen content. While the relationship is scattered (as indicated by the large error bars), it is quite clear that charging more DRI did not serve to decrease the tap nitrogen and may even be associated with an increase in nitrogen.

Also show in Figure 4.2 is a "dilution line" which shows the expected nitrogen content of the steel at tap, if the DRI contains zero nitrogen, and simply dilutes the other (nitrogen-containing) charge materials such as scrap. Such dilution is expected to be the main way in which DRI lowers tap nitrogen.[55] Dilution is assumed to follow a simple mass balance, given by equation 4.1:

$$[N]_{tap} = x_{DRI}[N]_{DRI} + (1-x_{DRI})\,[N]_{other} \qquad (4.1)$$

In this equation, $[N]_{tap}$ is the nitrogen content of the steel at tap, x_{DRI} is the mass fraction of DRI in the metallic furnace charge, $[N]_{DRI}$ is the nitrogen content of the DRI, and $[N]_{other}$ is the (average) nitrogen content of the non-DRI portion of the metallic charge. To calculate the dilution line in Figure 4.2, it was assumed that DRI contains zero nitrogen; the value of $[N]_{other}$ was chosen to match the observed average tap nitrogen content of 68 ppm with 55% of DRI in the metallic charge.

Evidently, adding more SL/RN does not give the dilution effect expected for nitrogen-free DRI. This observation is consistent with the hypothesis that the SL/RN contains nitrogen. Chemical analysis of DRI also supported this point, as shown in the next section.

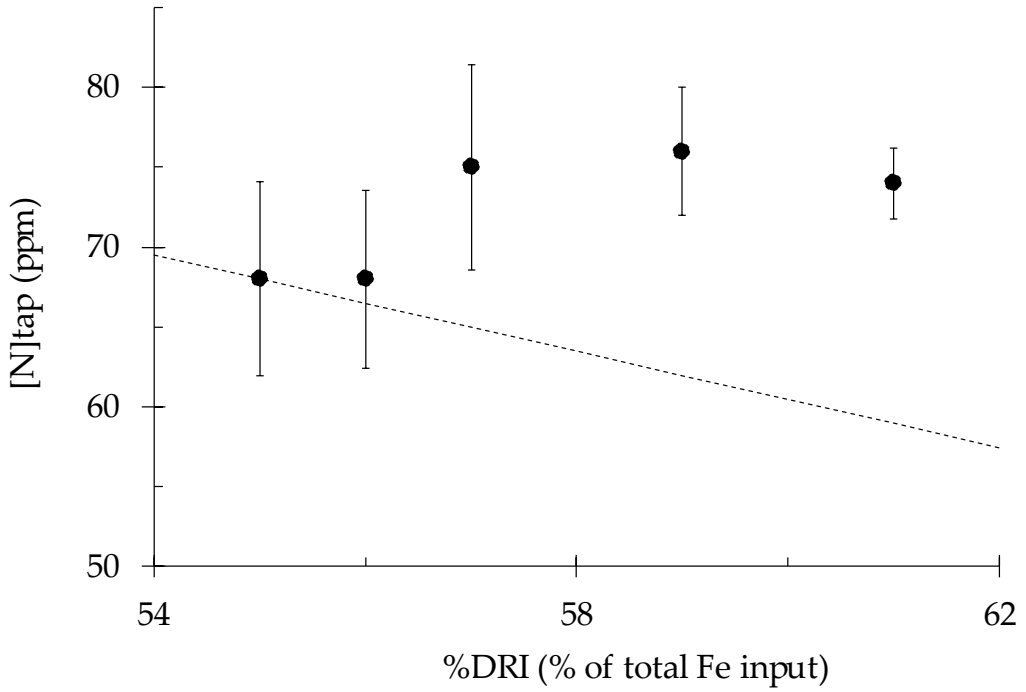

Figure 4.2: Nitrogen content of liquid steel after tapping from the electric arc furnaces. Samples for analysis were taken directly after tap, before dispatch to the ladle furnace. These are average values, for heats consisting of scrap and DRI only. The broken line shows the expected trend for the case where DRI simply dilutes the nitrogen within the steel melt. The error bars are the 95% confidence level on the mean nitrogen content achieved – this shows that there is, at least, statistically, a difference in the mean nitrogen content for the lowest (55% DRI) and highest (61% DRI) levels of DRI charged, implying that the argument that the nitrogen levels are lowered by dilution only is not valid in this case.

4.5. Nitrogen in DRI: Analyzed nitrogen content of SL/RN DRI

Nitrogen content of DRI: Experimental approach

Samples of SL/RN DRI were obtained from the plant (approx. 30 kg in total, from two kilns). The samples were split into smaller aliquots by cone and quartering, and subsequently screened into different size fractions (in the size range -25 mm to +212 μm) using a set of Tyler sieves. Aliquots were taken from each of the size ranges (again by cone and quartering). Each of these sub-samples was milled in a

swing mill. The nitrogen contents of the milled samples were determined by LECO (combustion) analysis.

Nitrogen content of DRI: Results

The SL/RN DRI contained significant concentrations of nitrogen (Figure 4.3). More than half of the size fractions contained more nitrogen than the target tap analysis of 80 ppm; the nitrogen content of all the size fractions exceeded the maximum nitrogen solubility in α-ferrite (which is around 50 ppm for pure iron in 1 atm of N_2; see Figure 4.4).

Figure 4.3 also shows that the nitrogen content of DRI fines is approximately 280 ppm (which happens to be approximately the maximum nitrogen solubility in austenite in 1 atm N_2; see Figure 4.4).

The analyzed nitrogen content of the SL/RN DRI supports the hypothesis that this material is a significant source of nitrogen in electric furnace steelmaking.

There is a clear dependence of nitrogen content on particle size, with generally lower concentrations of nitrogen in larger DRI particles (Figure 4.3). This may reflect a kinetic effect during nitriding of the DRI in the reduction kiln or rotary cooler: Larger particles would present a larger resistance to pore diffusion (of molecular nitrogen into the particles). The next chapter considers the expected nitriding kinetics.

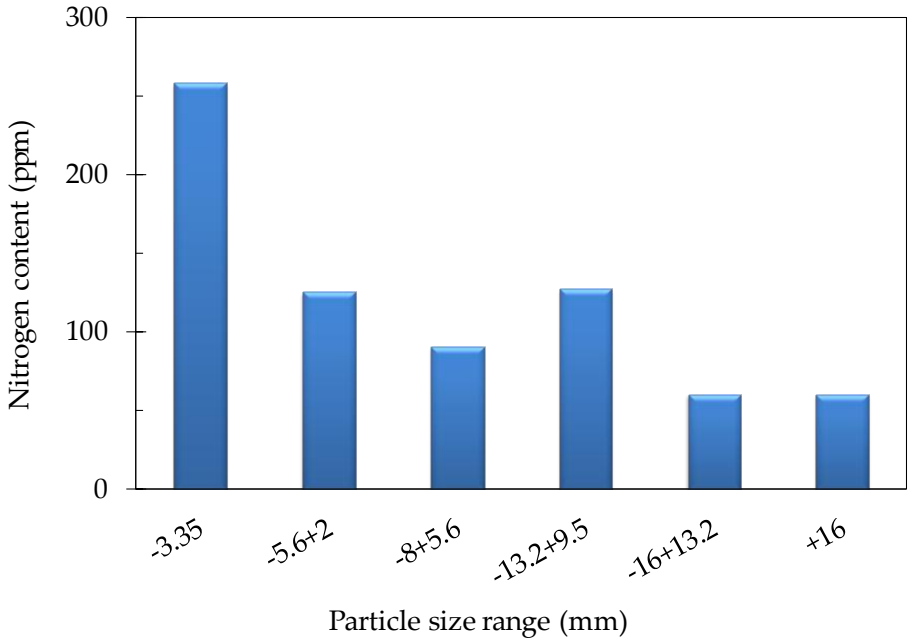

Figure 4.3: Nitrogen content of different size fractions of SL/RN DRI (Average [N] ~ 100 ppm for -5.6+13.2mm range)

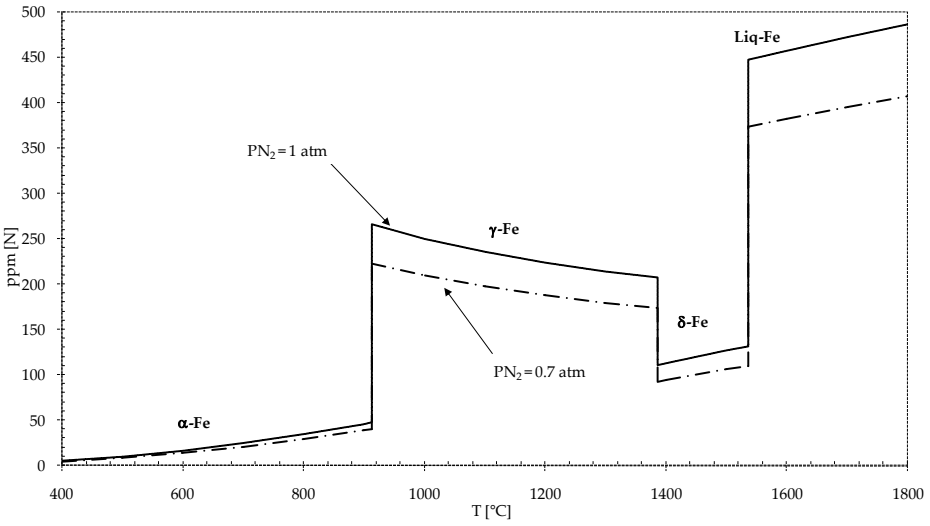

Figure 4.4: Solubility of nitrogen in iron (calculated with data from the Steelmaking Data Sourcebook[63].

4.6. Conclusion

Heats in an EAF where SL/RN DRI was charged in higher proportions (relative to scrap) did not lower nitrogen (as expected). Chemical analysis of DRI particles show significant levels of nitrogen (in most cases exceeding the solubility limit of nitrogen in iron at room temperature), which depends on particle size – it is suspected that this nitrogen is picked up in the SL/RN process, as shown in the next chapter.

Chapter 5:
Proposed mechanism of nitrogen pickup by SL/RN DRI: Mathematical prediction of nitriding time

The DRI particles show significant nitrogen pickup (as evidenced by Fig 4.3). In this section, a possible mechanism for nitriding of DRI particles is proposed. This chapter details the possible mechanism of nitriding as well as simple kinetic models to quantify each possible rate determining step (during nitriding of DRI).

There are at least two possible sources of the nitrogen in the DRI:

Main source: Penetration of nitrogen gas into the bed, when DRI is cooling:

Nitrogen gas diffusion into the porous DRI particles can cause nitriding. During reduction in the rotary kiln, the solids bed is continuously flushed by CO (reaction product), and no nitrogen pick-up is expected. However, the reduction rate rapidly decreases once the DRI is cooled (upon transfer to the rotary cooler), causing CO production to cease and allowing nitrogen to diffuse into the solids bed and into the individual DRI particles. It is hence thought that nitriding of the DRI particles occurs during cooling in the rotary cooler, where the flow of CO from the bed is not sufficient to shield the DRI from nitrogen present in the cooler atmosphere. An estimate was made to test the idea that nitrogen is picked up during cooling, by estimating how much nitrogen would penetrate into the solids bed, for different areas within the kiln and/or cooler.

Alternative/Parallel source:

Since coal contains small amounts of nitrogen (the average nitrogen content of all coals listed in the US Geological Survey Coal Quality Database, version 2.0[43], August, 2004 is 1.3% by mass (dry basis)). Ultimate analyses on South African coals aren't as widely published, but one figure[44] was found, ~2%). When the coal is devolatilized, N-containing gas species are released and might nitride iron. Studies[45] show that nitrogen can be released as $HCN_{(g)}$, which can give nitriding similar to molten cyanide salts. However, the small amount of nitrogen released in this form from coal would be diluted by other gases in the kiln and would also need to be in contact with iron (and not iron ore) long enough at temperature for nitriding to occur. Volatile release is expected to occur while the solids are heating up[58] before metallic iron has formed. Hence nitrogen from coal is not expected to be a significant source of the nitrogen in the SL/RN DRI and is not considered further in this work.

5.1. Background to the process and initial assumptions for kinetic model

SL/RN DRI at the plant in question is produced in a rotary kiln as described in section 4.3. The kiln(s) in question produce 480-550 t of DRI per day at an ore/DRI ratio of 1.52.

A schematic of the kiln/cooler setup is shown in Figure 5.1.1 below.

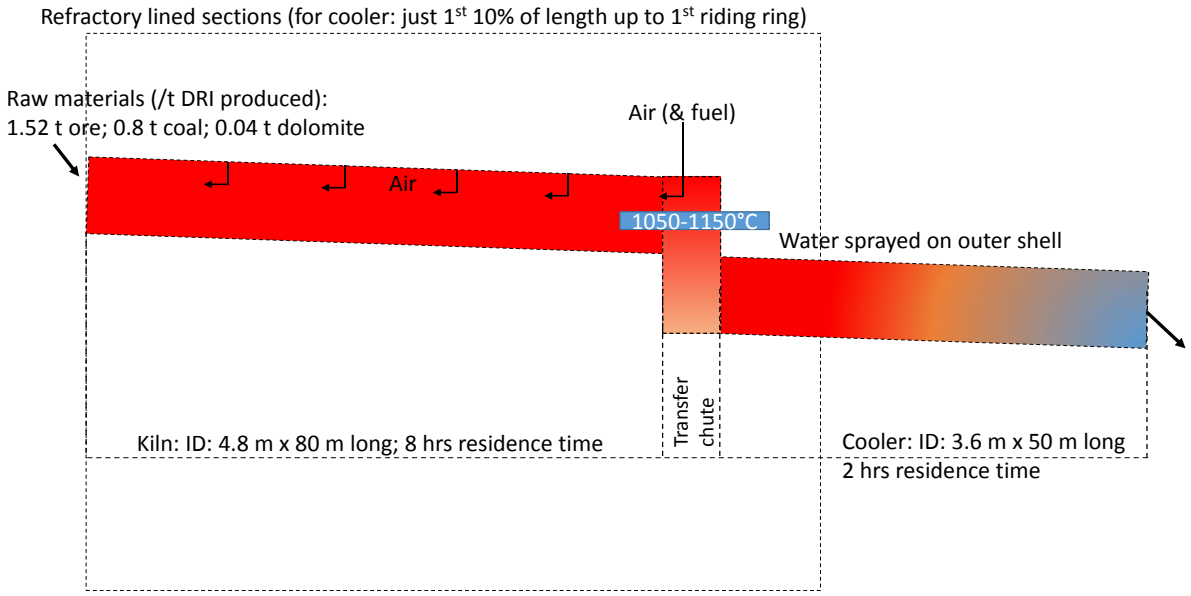

Figure 5.1.1: Schematic of the kiln-cooler setup at the plant in question (not to scale).

The rotary kiln (80 m long with an internal diameter of 4.8 m) is charged with iron ore, coal and dolomite and rotates at 0.4 rpm. Air is injected into the kiln in the freeboard of the kiln to provide heat for the strongly endothermic reaction between iron oxide ore and coal (carbon) to form solid DRI particles. The reduction process produces CO gas which, in turn, is combusted in the freeboard to form CO_2. The resultant atmosphere in the freeboard is one of principally CO_2, N_2 and water vapour. The DRI product is discharged into a rotary cooler (50 m long with an internal diameter of 3.6 m) via a transfer chute. In the cooler, the DRI is cooled using water that is sprayed on the outside of the steel shell. An induced draft fan ensures that a small positive pressure is maintained inside the kiln and cooler (to avoid air from the outside to penetrate the setup and cause re-oxidation of the hot DRI).

The discharge temperature of the DRI at the kiln end is roughly 1050-1150°C. Since the DRI is very hot and falls through the transfer chute, roughly 5 of the 50 meters of the cooler is lined with refractory material (similar to that inside the rotary kiln) to protect the steel shell of the cooler. The low thermal conductivity of the refractory material limits cooling in this part of the cooler, causing the temperature of the DRI to remain relatively constant, whereafter it starts cooling once it comes into contact with the water-cooled steel shell. Lifter bars are located along the length of the cooler

which is not refractory-lined, aiding cooling of the DRI along the other 45 meters to roughly 100°C (the cooling process takes ca. 2 hours in total).

To quantify the rate at which DRI particles are nitrided, a few assumptions were made regarding the atmosphere of the freeboard of the kiln and cooler, as well as the temperature and speed of the DRI particles (see Table 5.1.1):

Table 5.1.1: Assumed values for kiln and cooler used for the kinetic model(s)

Parameter	Rotary Kiln	Rotary Cooler	Justification for assumption
Rotational speed (rpm)	0.4	1	Actual plant data
Degree of fill (average)	0.2		
Length of unit (m)	80	50	
Inside diameter (m)	4.8	3.6	
Bed porosity / Void fraction (ε) - approximated by assuming DRI as a stack of spheres with random packing (packing density ~ 0.6)	0.4		
Atmospheric pressure Vanderbijlpark (1512 m above sea level), atm	0.84		
Freeboard nitrogen content (P_{N_2}), atm	0.55		Calculated based on pressure & air composition and assuming that all CO is combusted to CO_2 in the kiln.
Freeboard nitrogen content (X_{N_2})	0.65		
Temperature of DRI at discharge end of kiln and in first section of cooler where there is a refractory lining	1000 °C		Plant discharge temp at kiln exit 1050-1150°C. In this temperature range austenite is the stable form of iron.
Pore diffusion coefficient. D_e	6.23×10^{-4} m²/s		For Binary mixture of N_2 and CO_2. See section 5.3.

Possible rate limiting steps during the nitriding of DRI particles in the kiln/cooler

The rate at which nitriding occurs can be limited by (see Figure 5.1.2):

1. Mass transfer of nitrogen gas from the freeboard into the bed of the kiln/cooler as well as entrainment of gas into the bed;
2. Diffusion of molecular nitrogen through the pores of the DRI particles;
3. Dissociation of pure nitrogen on the surface of solid austenite;
4. Solid state diffusion of nitrogen into iron (in DRI particles).

The time (or concentration profile with time) for each step was evaluated and the results plotted.

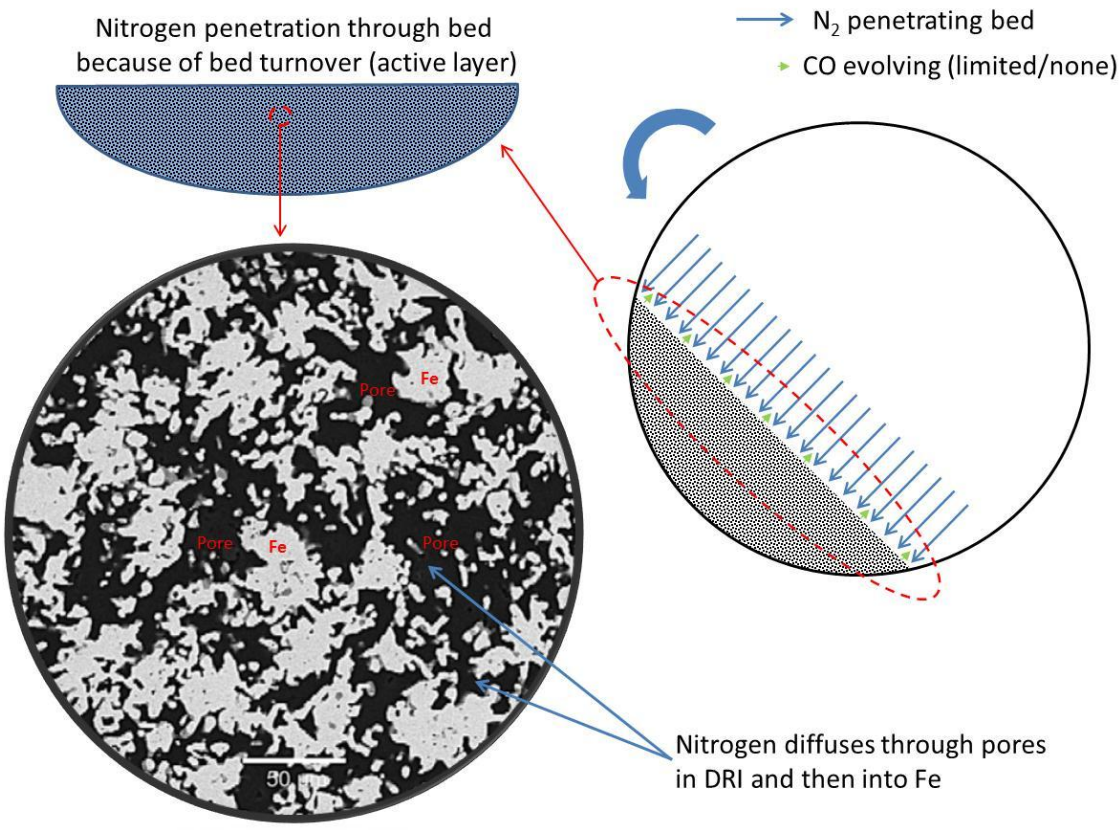

Figure 5.1.2: Schematic of the possible rate limiting steps during nitriding of iron.

5.2. Mass transfer of nitrogen from the freeboard to the solids bed in the kiln and cooler, with subsequent entrainment of gas into the bed

This section describes the evaluation of the following question: can nitrogen penetration (and entrainment) into the solids bed in the kiln or cooler be the rate limiting step for nitriding of DRI particles?

Approach:

a. *Calculate the composition of the gas is that might penetrate the bed;*
b. *Calculate the rate at which nitrogen gas can be entrained by the bed;*
c. *Calculate whether the rate of nitrogen transport is high enough for the mass flow rate of DRI through the unit (cooler) – i.e. that the reaction cannot be "starved" by a low gas flow/entrainment value;*
d. *Calculate whether the entire bed of material is exposed to enough gas for nitriding to occur;*
e. *Calculate the rate of nitriding of DRI particles if gas transport is not rate limiting*

Composition of the gas in the freeboard that can penetrate the solids bed

The gas composition of the freeboard of the kiln and cooler is approximately the same: within the kiln, O_2 (as air) is injected to combust CO gas (from the reduction process) to form CO_2 by the reaction: $CO + ½ O_2 = CO_2$. Consequently, the atmosphere above the solids bed (in the reduction zone where nitriding of DRI particles might be possible) is one of CO_2 and N_2 (with some water vapour, ignored for the calculations made in table 5.1.1). An induced draft fan is used to maintain a slight positive pressure through the kiln and cooler (to avoid air ingress from the outside which could re-oxidise the hot DRI), hence the off-gas in the freeboard of the kiln is transported to the rotary cooler, where no CO gas is evolved.

Within the solids beds of each unit, the gas composition is different: within the kiln, in the reduction zone, where iron oxide is reduced to iron, CO gas is evolved from the solids bed and the composition of gas (CO/N_2 ratio) within the bed is a strong function of the rate of CO evolution. Within the cooler, there is no gas evolution and the composition is hence one of N_2 and CO_2. For both the cooler and the rotary kiln, gas, the same as the freeboard will be entrained from the freeboard into the bed at a certain rate (estimated later in this section).

At the surface of the solids bed in the cooler, the mole fraction of nitrogen will be equal to that of the freeboard, $X_{N2} = 0.65$ (Since air contains roughly 79% N_2 and 21% O_2, by volume, if it is assumed that all of the CO formed within the bed is combusted to CO_2 with half a mole of O_2 per mole CO_2 formed, the resultant gas will contain an amount, in mole fraction, of $79/(79+2*21)=0.65$ N_2).

Rate at which nitrogen penetrates the solids bed

An initial approximation of the relative depth of penetration of nitrogen into the solids bed (for the kiln and cooler), if it were static, was made following the dusty gas approach by Tien and Turkdogan[57]. The result of this is shown in Appendix A.1. The situation in the rotary kiln and cooler, however, is different and is a slightly more complex mass transfer problem, involving movement of the solids bed.

Mass transfer in rotary kilns has been studied by only a few authors[e.g.46,47], since most rotary kiln processes are heat transfer limited. In this project, the work of Heydenrych et al[46] as well as Ferron et al[47] was used to approximate some of the mass transfer rates within the solids bed for each unit.

Consider the hypothetical cross section of a rotary unit in Figure 5.2.1

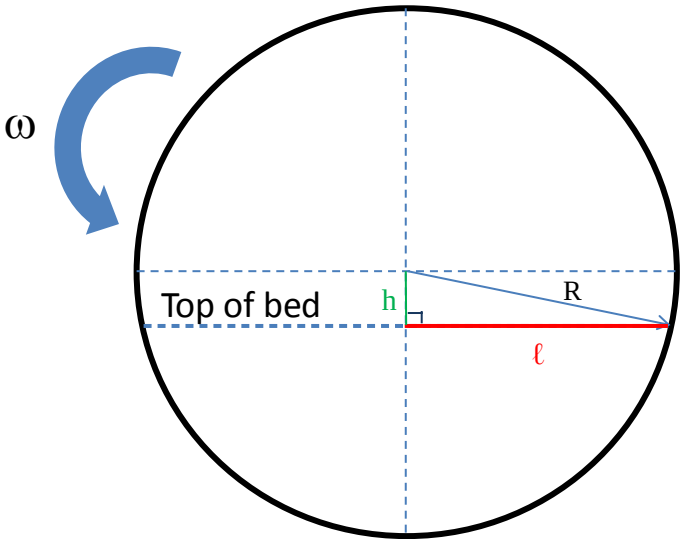

Figure 5.2.1: Cross-section of the rotary units (not to scale).

For the variables defined in Figure 5.2.1, Heydenrych et al[46] found the volumetric flow rate, Q_i (m^3/s) of gas that could be entrained by the bed to be:

$$Q_i = \tfrac{1}{2}\varepsilon\omega L(R^2-h^2)$$

where ε is the bed voidage, ω is the angular velocity, L is the total length of the unit in the axial direction (m), R is the radius of the vessel (m) and h is the perpendicular distance from the radial centre of the kiln bed to the bed surface (m).

The molar flux, J_{N_2} (mol/m^2s) of nitrogen gas into the bed is given by:

$$J_{N_2} = \frac{Q_{N_2}}{2L\ell}\frac{P_{N_2}}{RT}$$

where L is the total length of the unit (m), ℓ is the horizontal width of the bed (m), P_{N_2} is the partial pressure of nitrogen in the freeboard (Pa), R is the universal gas constant (8.314 $J.mol^{-1}K^{-1}$) and T absolute temperature (K).

The value of Q, inside the rotary kiln and cooler, based on the conditions stated in Table 5.1.1 is 2.93 m^3/s and 2.57 m^3/s respectively.

Based on a simple mass balance, the mole fraction of nitrogen in the active layer, at a position, x (distance from discharge end in m), is then:

$$X_{N_2}^{kiln}(x) = \frac{J_{N_2}^{kiln}(x)}{\frac{J_{N_{2x}}^{kiln}(x)}{X_{N_2}^{freeboard}} + J_{CO}^{kiln}(x)}$$

where $J_{CO}^{kiln}(x)$ refers to the rate of CO evolution (in mol/m²s) at any position x. The value of $J_{CO}^{kiln}(x)$ was estimated by assuming the reduction profile of a similar kiln (in particular, the Griffith kiln on which the mathematical model of Venkataswaran and Brimacombe[58] of the SL/RN rotary kiln is based).

Using the reduction profile (shown is Figure 5.2.2), the fractional reduction, dF/dx (unit: (mass fraction FeO_x reduced)/m can be calculated. The rate (dn_{co}/dt, in mol/m³s) at which CO gas leaves the bed is then:

$$\frac{dn_{co}}{dt} = \frac{dF}{dx}\frac{v_{linear}\rho'_{Fe}}{1.5M_{Fe}}$$

where v_{linear} is the linear speed of the material moving through the kiln (production rate x ρ_{Fe}/A_{bed} where A_{bed} is the cross sectional area of the bed – unit for linear speed is m/s; the production rate was assumed at 515 t/day); ρ'_{Fe} is concentration density of iron, 763 kg/m³); M_{Fe} is the molar mass of iron and 1.5 the molar ratio of O to Fe in the ore (in this case assumed to be Fe_2O_3). This rate (in mol/m³s) can now be used to calculate the molar flux, $J_{CO}^{kiln}(x)$ of CO from the bed:

$$J_{CO}^{kiln}(x) = \frac{dn_{co}}{dt}V(x)\Big/_{2\ell\Delta x}$$

where V(x) is the average bed volume from which the flux occurs, $2\ell\Delta x$ is the transverse area element from which the flux occurs.

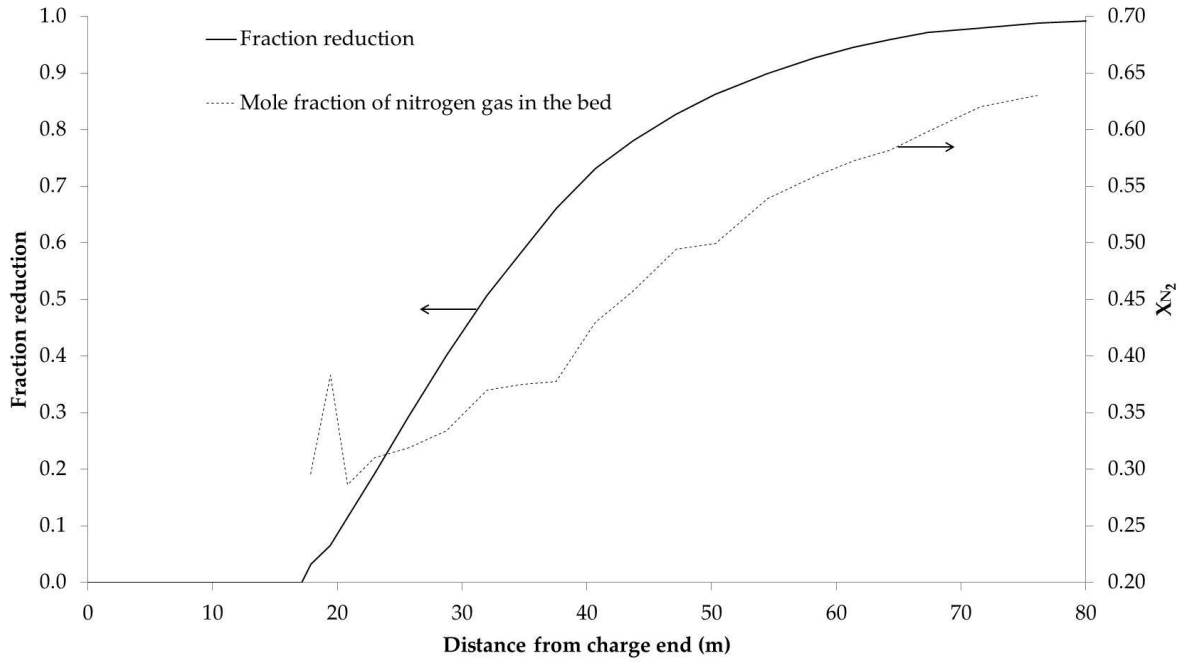

Figure 5.2.2: Reduction profile (solid line) and partial pressure of nitrogen gas (dashed line) for the rotary kiln.

The calculated mole fraction of nitrogen in the active layer within the kiln is low (when compared to the cooler where it is 0.65), reaching a maximum of ca. 0.6 only at the discharge end of the kiln (see Figure 5.2.2). In the pre-heating zone, the presence of nitrogen is insignificant, as no iron is present to take up nitrogen. It is therefore concluded that, relative to the cooler, there is very little nitrogen available for nitriding inside the kiln (although some nitriding might occur in the last few meters and that nitriding mostly occurs within the rotary cooler.

The section of the cooler where nitriding is most plausible is the first few meters of the cooler, where there is a refractory lining (in the case of this plant, the first 5 meters of the cooler): in this section the temperature of the DRI would be approximately constant (1000°C was assumed for all calculations) – the DRI would remain in this section for ca. 10-15 minutes (total residence time in the cooler is 2 hours).

For these conditions at the cooler entrance (1000 °C, $X_{N_2} = 0.65$, which makes $P_{N_2} = 0.55$ atm), the solubility limit of nitrogen in DRI (which is assumed to be iron, at this temperature austenite) is 186 ppm (as calculated by Sieverts' law, mentioned earlier in this document).

Calculation of whether the rate of nitrogen transport is high enough for the mass flow rate of DRI through the unit (cooler)

With the volumetric flow rate of nitrogen that is transported into the solids bed of the cooler known, an evaluation can be made whether enough nitrogen gas is transported into the bed for a given flow rate of DRI (iron) (i.e. that the freeboard contains enough gas for nitriding of DRI at any given time), to give significant nitrogen pick-up.

The flow rate of DRI through the section of the cooler where nitriding is most likely to occur is 6 kg/s (based on the production rate of 515 t/day of DRI produced by the rotary kiln in question). The mass flow rate of nitrogen in the same section of the cooler is equal to 0.04 kg/s (this is 10% of the volumetric flow rate of nitrogen, Q = 2.57 m^3/s, that is entrained by the bed, since the section for nitriding is the first 5 meters of the total 50 meters of the cooler). The maximum attainable concentration of nitrogen in iron for this mass flow rate of DRI and nitrogen, would be 0.04 kg/s / 6 kg/s, i.e. 0.67%, which is much more than the solubility limit of nitrogen in austenite at 1000°C, as given by Sieverts' law (186 ppm).

Clearly, transport of molecular nitrogen into the active layer would not be rate-determining.

Calculation of whether the entire bed of material in the cooler is exposed to enough gas for nitriding to occur

For nitriding of DRI particles to occur, the particles must be exposed to the gas to react. In mass transfer (inside a rotary kiln) terms, the layer of particles that is exposed to gas (and where reaction occurs) is referred to the active layer.

The frequency at which the bulk of the material is transported to the top plane (where it can react), is known as the rotational turnover ratio (Ferron[47]) and is given by the number $V^* = (\ell/R)^2/f$. This is the number of times per revolution that a given particle is transported to the active layer.

A plot of the rotational turnover ratio versus the fraction filled is given in Figure 5.2.3.

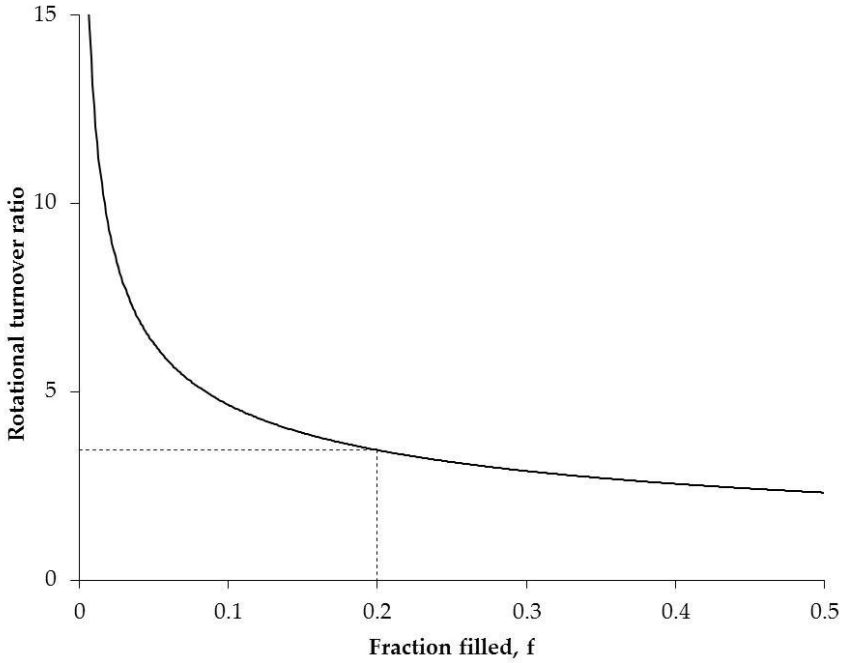

Figure 5.2.3: Rotational turnover ratio for rotary units[47].

For a fractional fill of 0.2, as in the cooler, the particles inside the vessel are turned over (and hence exposed to the gaseous atmosphere) 3.8 times per revolution as shown in Figure 5.2.3

The rate at which the active layer renews itself (i.e. where "fresh" particles are exposed to the gaseous atmosphere), N_P (particles/s), can be calculated by the following relationship (after Ferron[47]):

$$N_P = \frac{6(1-\varepsilon)\ell^2 L\omega}{d_P^3}$$

where ε is the void fraction of the bed, ℓ is the width of half of the top of the bed (horizontal cross section), L is the total length of the kiln/cooler, ω is the rotational speed (s^{-1}) and d_P the average particle diameter (in this case a value of 10 mm was assumed for all calculations).

The rate at which the active layer (i.e. layer where reaction occurs) in m^3/s is renewed is then:

$$\dot{V_{al}} = \frac{\pi}{6(1-\varepsilon)} d_P^3 N_P$$

It follows then, that the characteristic time it takes to renew the active layer, in seconds, τ_{al} is:

$$\tau_{al} = \frac{V_{bed}}{\dot{V}_{al}} = \frac{f\pi R_{cooler}^2 L_{cooler}}{\dot{V}_{al}} = \frac{f(R_{cooler})^2}{\omega \ell^2}$$

where f is the degree of fill of the cooler (0.2), R_{cooler} is the radius of the cooler (1.8 m) and L_{cooler} is the total length of the cooler (50 m). The value for τ_{al} is 2.5 seconds for the conditions quoted thus far.

If the solids bed is well-mixed, and if the rate at which iron is transported to the active layer determines the rate of nitriding, then the average nitrogen content of the bed would depend as follows on time: $[N] = [N]_{sat}(1-e^{-t/\tau})$ where $[N]_{sat}$ is the solubility limit of nitrogen in iron. Clearly, because τ is much smaller than the residence time in the first 10% of the cooler, transport of iron to the active zone is not rate determining either.

5.3. Pore diffusion of nitrogen through DRI particles

In this section, the possibility that diffusion of nitrogen through the pores of the DRI particles is the overall rate limiting step for nitriding was evaluated.

Approach:

Assume that the DRI particles are spherical, with outer radius r_o (see Figure 5.3.1) with an effective diffusivity D_{eff} (of N_2 in a N_2-CO_2 couple[48]) through the pores. Further assuming the particles are pure iron with a true density of 7.87 t/m³ and knowing the particle density thereof as ~3 t/m³, the particle porosity, ε_p can be calculated as $\varepsilon_p = 1-\rho/\rho_{Fe} \sim 0.6$ (where ρ is the particle density, i.e. moles of iron per volume of particle and ρ_{Fe} is the density of pure iron), and the tortuosity, τ_p as 1.15 with the correlation suggested by Wu et al[61].

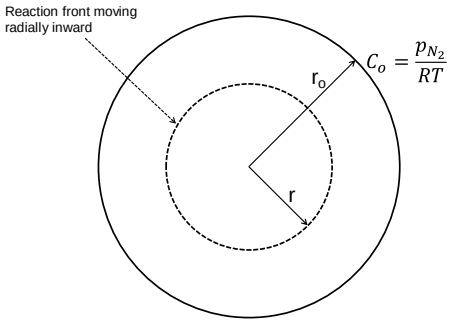

Figure 5.3.1: Schematic of the reaction front in a spherical iron particle (the concentration of nitrogen gas ahead of the reaction front is assumed to be zero).

Take the equilibrium nitrogen concentration in the iron to be q (mass fraction). Let X be the mole fraction of nitrogen in the gas.

For the case of pore diffusion control, a reaction front moves radially inward. Ahead of the front, the nitrogen concentration in the iron is zero, and behind the front the concentration is q.

Molecular nitrogen is transported to the reaction front in two ways: By pore diffusion, and by bulk flow of gas into the particle. Bulk flow occurs because nitrogen is removed from the gas phase when it dissolves in the particle. Assuming that the total amount of gas in the particle pores remains constant, the rate of nitrogen pick-up is simply equal to the bulk flow rate of gas into the pellet.

Let $\dot{n}$ be the rate of nitrogen pick-up. This is then given by:

$$\dot{n} = \dot{n}_{\text{diffusion}} + \dot{n}_{\text{nitrogen in bulk flow}} = \Delta C D_{\text{eff}} S + X\dot{n},$$

where ΔC is the concentration difference between the pellet surface and the reaction front, and S is the shape factor for diffusion into the pellet; $S=4\pi r_o r/(r_o-r)$ for the spherical geometry considered here.

Rearrangement gives $\dot{n} = \Delta C D_{\text{eff}} S/(1-X)$.

The concentration difference can be written in terms of the mole fraction of nitrogen in the bulk gas and the total pressure. If the initial nitrogen content in the iron is zero, the concentration of nitrogen in the gas at the reaction front is zero. The concentration difference is then simply equal to the nitrogen concentration at the outer surface of the pellet, which is given by:

$C_o = p_{N_2}/RT = Xp_{tot}/RT$, where p_{tot} is the total pressure (in Pa).

To calculate how the reaction front moves with time, an expression that gives how far the reaction front advances for a given amount of molecular nitrogen diffusion is required. The molar density of atomic nitrogen in the reacted pellet is $\rho q/M_N$, where M_N is the molar mass of atomic nitrogen (0.014 kg/mol). The rate at which the volume of the unreacted core changes is then given by:

$$-4\pi r^2 \frac{\mathrm{d}r}{dt} = \frac{2\dot{n}}{\rho q/M_N} = \frac{8\pi r_o r X p_{tot} D_{eff} M_N}{[(1-X)(r_o - r)RT\rho q]}$$

(the factor 2 is before $\dot{n}$ because 1 mole N_2 gives 2 moles of dissolved N)

Hence, separating variables:

$$\int -r(r_o - r)dr = \frac{2r_o X p_{tot} D_{eff} M_N}{(1-X)RT\rho q} \int dt$$

Using the boundary conditions that $r=r_o$ when $t=0$, and $r=0$ when $t=\tau$, integration yields:

$$\frac{1}{6} r_o^3 = \frac{2r_o X p_{tot} D_{eff} M_N}{(1-X)RT\rho q}\ \tau$$

The time for nitriding (in seconds) of the particle to a mass fraction of nitrogen, f, is then given by:

$$\tau_{pore} = \frac{(1-X)RT\rho q r_o^2}{12 X p_{tot} D_{eff} M_N} \qquad (5.2.1)$$

By using this expression, it was found, that pore diffusion is rapid for the entire size range in comparison to the other possible rate limiting steps. For example, the time for complete nitriding to occur (under pore diffusion control) is estimated to be 0.2s for particles with a radius of 0.01m.

5.4. Estimate of the degree of nitriding if nitrogen dissociation is rate limiting

For the case where nitrogen pick-up is limited by dissociation of molecular nitrogen on the iron surface, Grabke[49] showed that the rate of nitrogen pick-up by iron foil of thickness 2*L* is given by:

$$\frac{d[\mathrm{N}]}{dt} = \frac{kKM}{\rho L}\left([\mathrm{N}]_{eq}^2 - [\mathrm{N}]^2\right)$$

where k is the rate constant (in mol/s.m^2.atm), M is the molar mass of N_2 (0.028 kg/mol), ρ is the density of iron (7800 kg/m^3), $K = p_{N_2}/[\mathrm{N}]_{eq}^2$ is the equilibrium constant, [N] is the nitrogen content of the iron, expressed as a mass fraction, and $[\mathrm{N}]_{eq}$ is the equilibrium nitrogen content.

Separation of variables gives:

$$\int_0^{[\mathrm{N}]} \frac{d[\mathrm{N}]}{[\mathrm{N}]_{eq}^2 - [\mathrm{N}]^2} = \frac{kKM}{\rho L}\int_0^t dt$$

for the case where the iron initially contains no dissolved nitrogen.

Integration gives:

$$\ln\left(\frac{[\mathrm{N}]_{eq} + [\mathrm{N}]}{[\mathrm{N}]_{eq} - [\mathrm{N}]}\right) = \frac{2kKM[\mathrm{N}]_{eq}}{\rho L}t$$

For 1000°C, K=1.6×10^7 atm. According to Grabke, k=1.2×10^{-4} mol/s.m^2.atm at 1000°C, for the case where the gas contains no sulphur. Substitution of these values, using L=15μm and p_{N_2}=0.55 atm, gives the nitrogen pickup-curve (see next section); this illustrates that nitrogen pick-up should take 1-2 minutes, if dissociation is rate-determining. If the gas atmosphere has a significant sulphur potential, nitrogen pick-up would be significantly slower,[50] as illustrated by Figure 5.4.1.

The gas in the SL/RN process has a significant sulphur potential: sulphur pick-up by SL/RN DRI has been studied by Theron[51] and occurs via reaction of DRI with COS gas (formed by reaction of CO with S_2) in the temperature region 800-1000°C. Plant data shows that the DRI product contains ca. 110-150 ppm S.

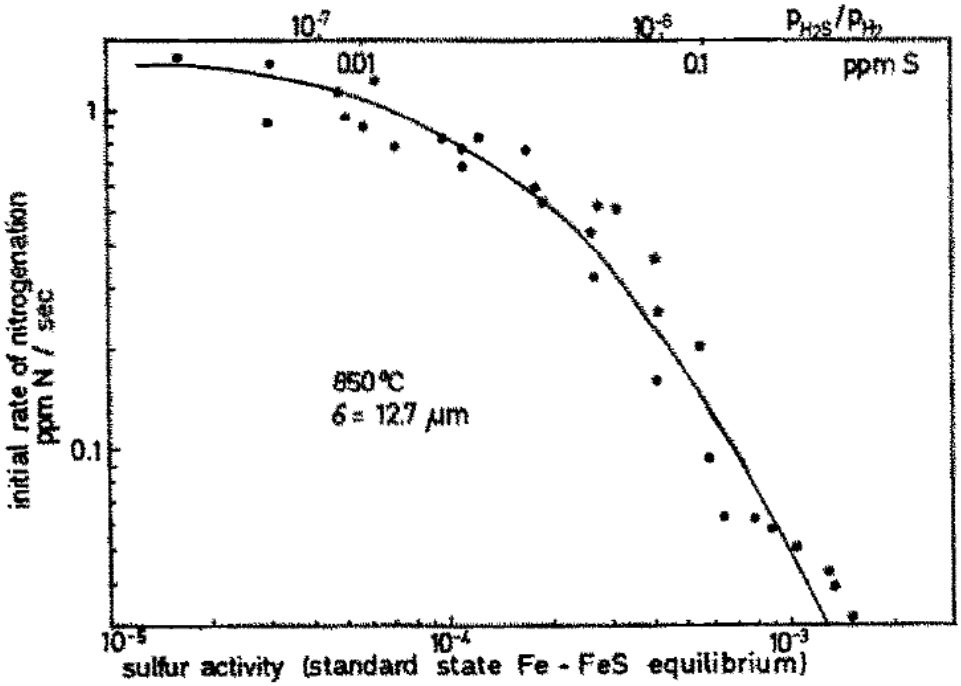

Figure 5.4.1: Effect of gas sulphur potential on the rate of nitrogen pick-up[50]

5.5. Estimation of solid-state diffusion of nitrogen into direct-reduced iron

The transient diffusion of atomic nitrogen in the solid state was estimated by considering the DRI pore walls as a 1D plane wall. Essentially, the calculation is a mass-transfer analogue to a transient heat transfer problem through a 1D plane wall[52].

The dimensionless centre concentration of nitrogen can be estimated analytically by:

$$\frac{X_0 - X_{surface}}{X_i - X_{surface}} = C_B e^{\left(-A_B^2 \frac{D_N t}{L^2}\right)}$$

$$C_B = \frac{4 sin A_B}{2A_B + sin 2A_B};\ A_B(tan A_B) = Bi_m = \frac{mL}{D_{N\ in\ \gamma}}$$

where X refers to the centre concentration of nitrogen in the DRI (austenite, γ) at any time t for a half-thickness, L, a surface concentration $X_{surface}$ and initial concentration X_i (in this case, 0 for t=0). Bi_m is the mass transfer Bi number, a dimensionless ratio of internal resistance to mass transfer by diffusion (i.e. internal transfer) to external mass transfer by convection (boundary layer transfer); m is the mass transfer coefficient. In this case $Bi_m \rightarrow \infty$ (diffusion controlled reaction), hence $A_B = {}^{\pi}/_{2}$ and $C_B = {}^{4}/_{\pi}$. D_N refers to the diffusion coefficient of nitrogen in austenite (m^2/s).
Polished sections of typical DRI particles were made, to determine the value of L for all calculations using a backscattered electron image on a scanning electron microscope for imaging and measuring the length of several DRI "arms". It was

found that the value was between 13 and 20 micron (results of measurements shown in Appendix 1). A value of 15 micron was used for all calculations. A typical backscattered image is shown in Figure 5.5.1.

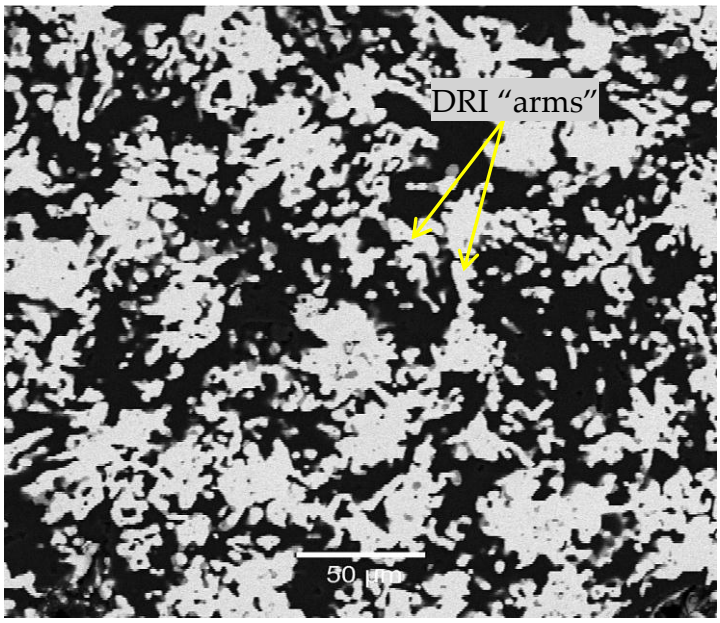

Figure 5.5.1: Backscattered electron image of DRI "arms" in a typical DRI particle through which nitrogen must diffuse in the solid state.

The dimensionless off-centre concentration of nitrogen at a position x, is given by:

$$\frac{X - X_{surface}}{X_0 - X_{surface}} = cos\left(\frac{A_B x}{L}\right)$$

And hence the concentration of nitrogen at any fractional depth (x/L) can now be calculated at any time, t:

$$X = X_{surface}\left[1 - \cos\left(\frac{A_B x}{L}\right) C_B e^{\left(-A_B^2 \frac{D_{N\ in\ \gamma} t}{L^2}\right)}\right]$$

The concentration of nitrogen, then, with time (if no other step is rate limiting, but solid state diffusion) is thus:

$$[N] = 10^5 K \sqrt{P_{N_2,freeboard}}\left[1 - \cos\left(\frac{A_B x}{L}\right) C_B e^{\left(-A_B^2 \frac{D_{N\ in\ \gamma} t}{L^2}\right)}\right]$$

where K is the equilibrium constant for the nitrogen dissociation constant (from Sieverts' law). For 1000 °C, the value for K=0.025 (See section 3.2).
The value of D_N (in this equation the unit is cm^2/s) was estimated using the average composition independent equation given by Bakker[53]:

$$D_N = 0.91e^{-\frac{168560}{RT}}; with\ T\ in\ K\ and\ R = 8.314\ J/molK$$

The time constant for solid-state nitriding is then given by: $\tau = \frac{4L^2}{\pi^2 D_N}$. Substitution of L=15x10^{-6} m and 1.1x10^{-11} m²/s gives τ=8.3 seconds.

5.6. Estimate of the degree of nitriding of DRI particles for each step

The degree of nitriding of DRI particles can be best expressed by dividing the concentration of nitrogen in the DRI particle by the maximum attainable concentration (i.e. maximum solubility of nitrogen in austenite at 1000°C, with P_{N_2} =0.65 atm), for each rate limiting step as a function of time, since the characteristic time for each step is known. Figure 5.6.1 nitrogen dissociation at the DRI surface is the slowest step during nitriding.

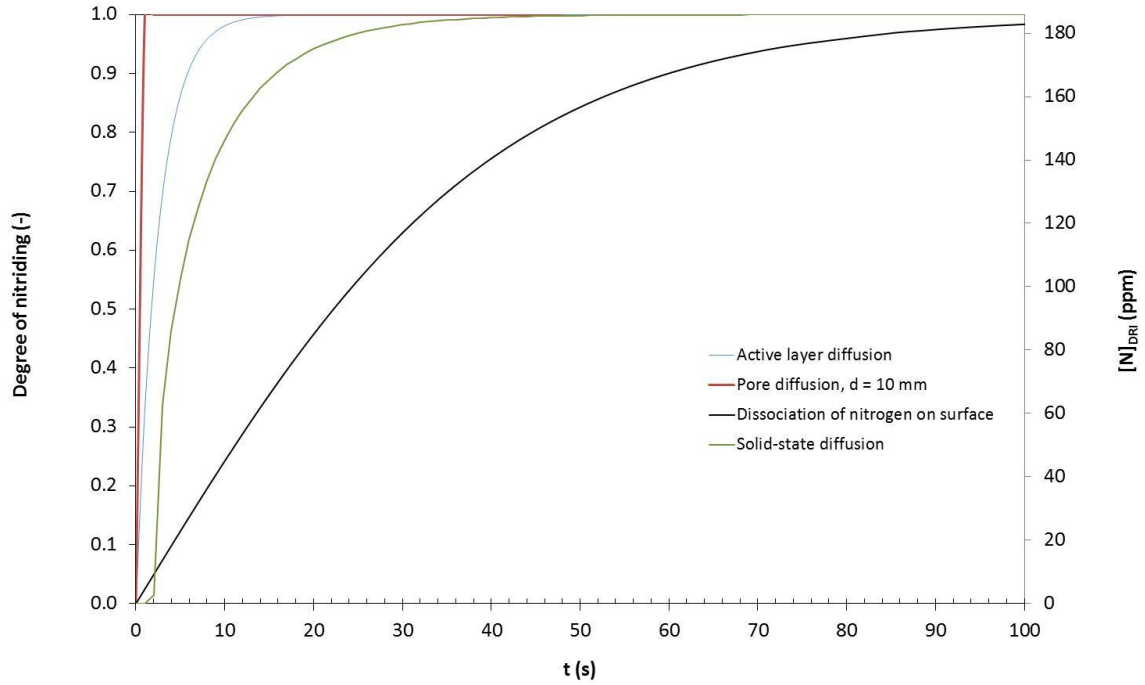

Figure 5.6.1: Degree of nitriding of DRI particles for active layer-; pore- or solid-state diffusion control; as well as where nitrogen dissociation on the surface is rate limiting. A particle size of 10 mm is typical (as a 80% passing size) for the plant in question. For solid state diffusion, the a value of x/L = 0 was chosen (i.e. nitrogen diffusion right through to the middle of the DRI "arm"). The nitrogen content corresponding to the degree of nitriding in shown on the right hand axis. Dissociation of nitrogen at the iron surface seems to be the most plausible rate limiting step.

For particles that spend roughly 10-15 minutes in the "nitriding zone" (first 10% of the length of the unit) of the cooler, it is quite possible to pick up nitrogen.

The most plausible rate limiting step is that of nitrogen dissociation onto the DRI surface, since it has been shown, by calculation, to be the slowest. This step can also be further retarded by the presence of sulphur.

5.7. Conclusion

The main conclusion of this chapter is that each of the possible rate limiting steps for nitrogen pickup by DRI particles can be quantified and shows that nitrogen pickup is expected to be rapid within the section of the cooler where a refractory lining exists (this is the first 10% of the length of the cooler). This is a small "window of opportunity", but one which is important with respect to nitrogen pickup. The most plausible rate limiting step is that of nitrogen dissociation onto the DRI surface.

Chapter 6:
Relationship between tap nitrogen content and melt-in carbon content of Electric Arc Furnace steel: plant observations and statistical predictions

The previous chapter has shown the feasibility of the proposed mechanism by which direct-reduced iron picks up nitrogen in the rotary cooler (of the SL/RN process). It hence appears inevitable that the direct-reduced iron would transfer nitrogen to the steel bath in the electric arc furnace. Because the direct-reduced iron does not contribute to nitrogen control, another approach is necessary to achieve reliably low nitrogen contents in tapped steel. Evolution of carbon monoxide ("carbon boil") is known to be one such mechanism. This chapter evaluates plant data, to address two main questions:

1. Whether higher melt-carbon correlates with lower tap nitrogen contents.
2. Whether the quantitative relationship between melt-in carbon and nitrogen at tap can be used to control tap nitrogen contents.

6.1. Relationship between melt-in carbon and final nitrogen content

Data from 3120 heats are shown in Figure 6.1. Analysis from all heats of the three EAFs were included, with no filtering of the results: heats with hot metal were included (since these heats have higher melt-in carbon contents), and the small number of unfeasibly low tap nitrogen analyses (less than 40 ppm were also not filtered). See Figure 4.1 for the time at which the melt-in carbon was measured.

No relationship is apparent in Figure 6.1, because of the scatter of these data from practical industrial production. To reveal the underlying relationship, summary statistics were calculated. Figure 6.2 shows the relationship between average tap nitrogen content (with a 95% confidence interval), as a function of melt-in carbon. This figure was generated by binning the different melt-in carbon contents.

Figures 6.2 (a) and (b) show two important effects: First, higher melt-in carbon contents are indeed correlated with lower tap nitrogen contents (on average); the relationship is a semi-logarithmic one. Second, it is possible to achieve average tap nitrogen contents below 50 ppm if the carbon content at melt-in is 0.3% C or higher. However, given the wide scatter in tap nitrogen contents, higher melt-in carbon contents would be required to ensure that **most** heats (rather than just average heats) have low tap nitrogen contents. The statistical basis for predicting the distribution in tap nitrogen contents is presented later in this chapter.

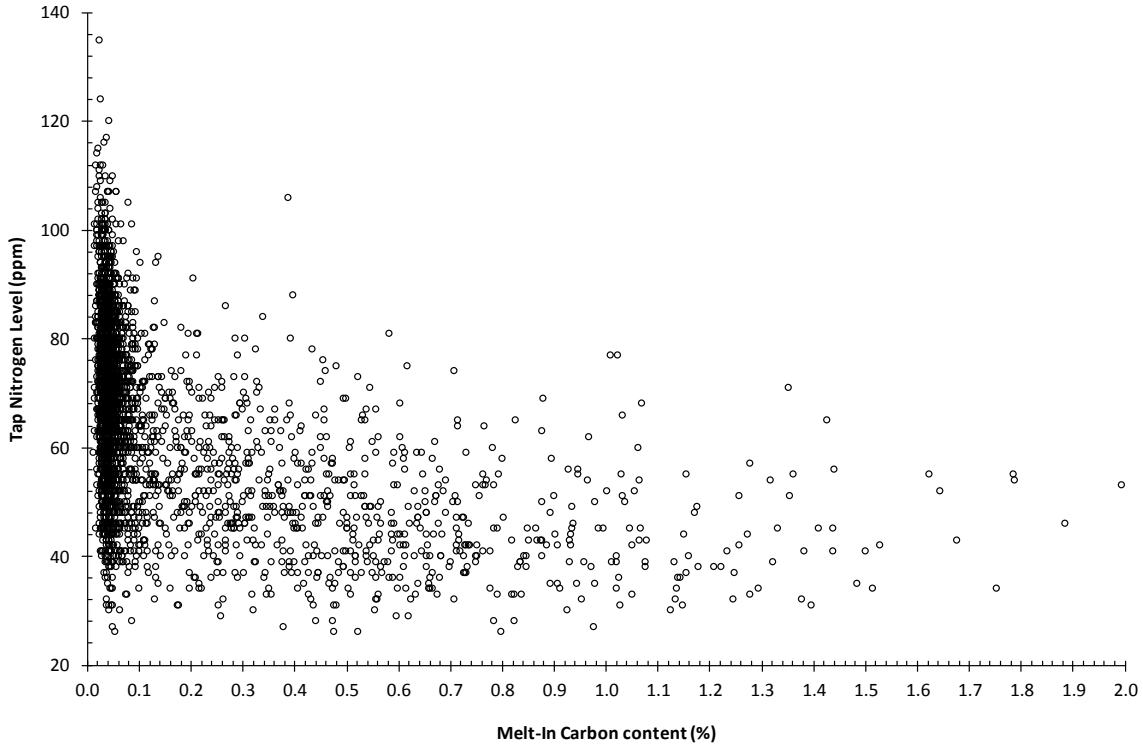

Figure 6.1: Scatter plot of Nitrogen content at tap as a function of Melt-In Carbon content.

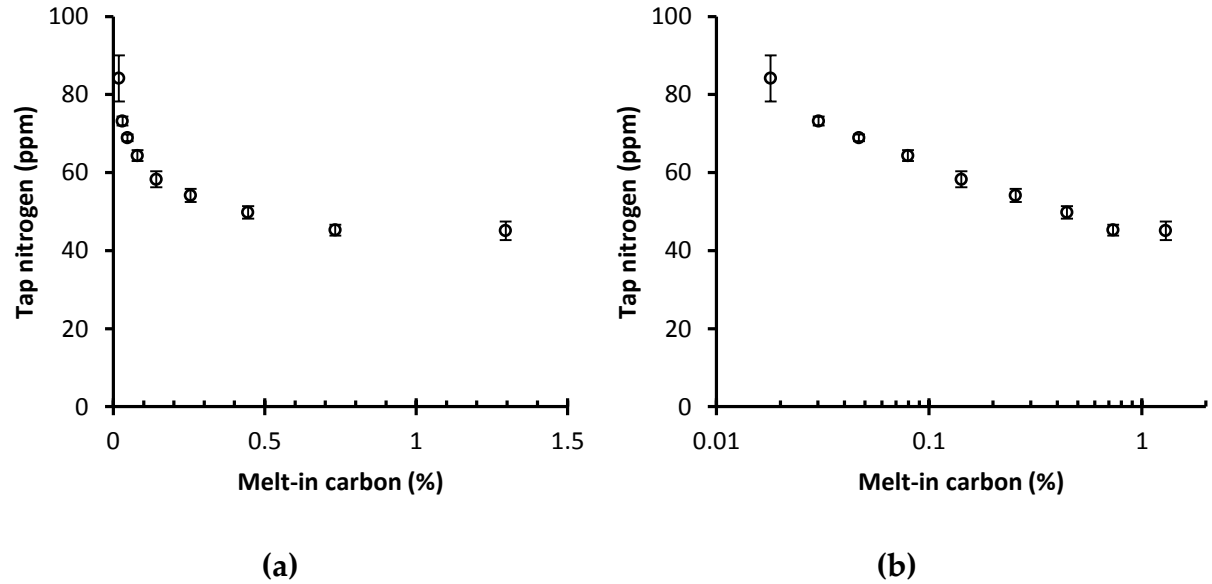

Figure 6.2: Average nitrogen content of tapped steel as a function of melt-in carbon (grouped data) – (a) carbon on a linear scale, (b) carbon on a semi-logarithmic scale.

6.2. Possible origin of observed relationship between tap nitrogen and melt-in carbon

Several processes affect the tap nitrogen content: direct reduced iron carries nitrogen into the metal bath; carbon monoxide flushes nitrogen out of the bath; nitrogen from air ingress can dissolve into the steel (especially if the nitrogen dissociates in the arc).

It would be helpful to be able to predict tap nitrogen content based on quantification of each of these processes.

As a first attempt to identify the main rate-determining step, the maximum possible degree of removal of nitrogen by carbon monoxide can be calculated; this maximum rate corresponds to the case where CO bubbles leave the steel melt saturated with nitrogen. This is similar to the approach used by Turkdogan[13] to calculate the "maximum rate of degassing of liquid steel".

At saturation, the partial pressure of nitrogen in the gas bubbles is given by:

p_{N_2} = (ppm N / K)^2, where K = 450 for 1600°C. In this expression, it is assumed that the Henrian activity coefficient of dissolved nitrogen is f_N=1.

The (maximum) rate of nitrogen removal from the steel bath is then:

$dm_N/dt = -(p_{N_2} / p_{tot}) N_{gas} M_{N_2}$,

where p_{tot} is the average pressure in the bath, N_{gas} is the molar flow rate of gas, and M_{N_2} is the molar mass of nitrogen.

Also, $dm_N/dt = 10^{-6} W_{steel} d(\text{ppm N})/dt$, where W_{steel} is the steel mass.

Substitution gives:

$10^{-6} W_{steel} d(\text{ppm N})/dt = -(\text{ppm N})^2 N_{gas} M_{N_2} / (K^2 p_{tot})$

Integration gives:

$1/(\text{ppm N}_o) - 1/(\text{ppm N}) = -10^6 N_{gas} t M_{N_2} / (W_{steel} K^2 p_{tot})$

The total number of moles of gas generated per steel mass ($N_{gas} t/W_{steel}$) depends on the amount of carbon removed as follows:

$N_{gas} t/W_{steel}$ = [%C]/(100 M_C), where M_C is the molar mass of carbon.

Since nearly all the carbon in the steel is removed during steelmaking, the amount of carbon removed can be taken to be approximately equal to the melt-in carbon content.

Substitution gives:

$1/(\text{ppm N}) - 1/(\text{ppm N}_o) = 10^4$ [%C] $M_{N_2} / (M_C K^2 p_{tot}) = 0.077$ [%C]
(assuming total pressure of 1.5 atm)

The predicted dependence of tap nitrogen content on melt-in carbon, for the case of nitrogen saturation in the CO bubbles, is compared in Figure 6.3 with the actual behaviour. In calculating the predicted line, the initial nitrogen content was taken to be 90 ppm, to match the average tap nitrogen for the lowest melt-in carbon contents.

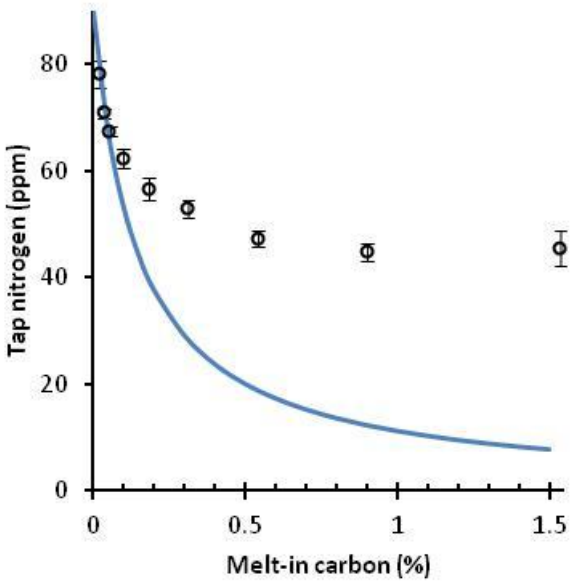

Figure 6.3: Predicted nitrogen tap content of liquid steel as a function of melt-in carbon content (solid line) compared to melt nitrogen and carbon analyses from three EAFs.

Clearly the actual tap nitrogen is significantly higher than the predicted value for nitrogen saturation in the evolved carbon monoxide. The difference may be due to the following:

1. Continued pick-up of nitrogen by the steel bath during steelmaking. The simple calculation assumes that no further nitrogen enters the steel after melt-in; nitrogen pick-up from the arc or from roof feeding of DRI would invalidate this assumption.
2. Kinetic limitations (whether mass transfer of nitrogen in the bath, or the rate of the interfacial reaction) would also decrease the extent of nitrogen removal.

In the absence of detailed information on bubble size and the kinetics of decarburization, it is not feasible to quantify the effects of continued nitrogen pick-up and kinetic limitations. Rather, the approach used here was not to make fundamental kinetic predictions, but instead to analyze the heat data statistically, to identify melt-in carbon contents which would yield tap nitrogen contents with defined probability.

6.3. Statistical evaluation of tap nitrogen contents

A useful interpretation of the tap data, which can be used at plant-level, is to evaluate the probability that the nitrogen level at tap would be below a pre-determined value, based on the melt-in carbon analysis. To determine such a probability, the relevant probability distribution of the nitrogen data was assumed to be normal.

Testing for normality can be done in various ways, most common (beyond simply drawing a histogram) is the use of probability plots and employing the Anderson-Darling Test[54]. The latter test is a goodness-of-fit test, in this case employed to test the hypothesis of whether each subset of nitrogen tap data differs significantly from a normal distribution (or not).

To draw probability plots (for the entire data set as well as the subsets, grouped on average carbon content), Minitab version 16.1.1 was used (set to a 95% level of confidence, as for the graphs). Figure 6.4 shows an example of the typical output from Minitab for a set of (normal) probability plots.

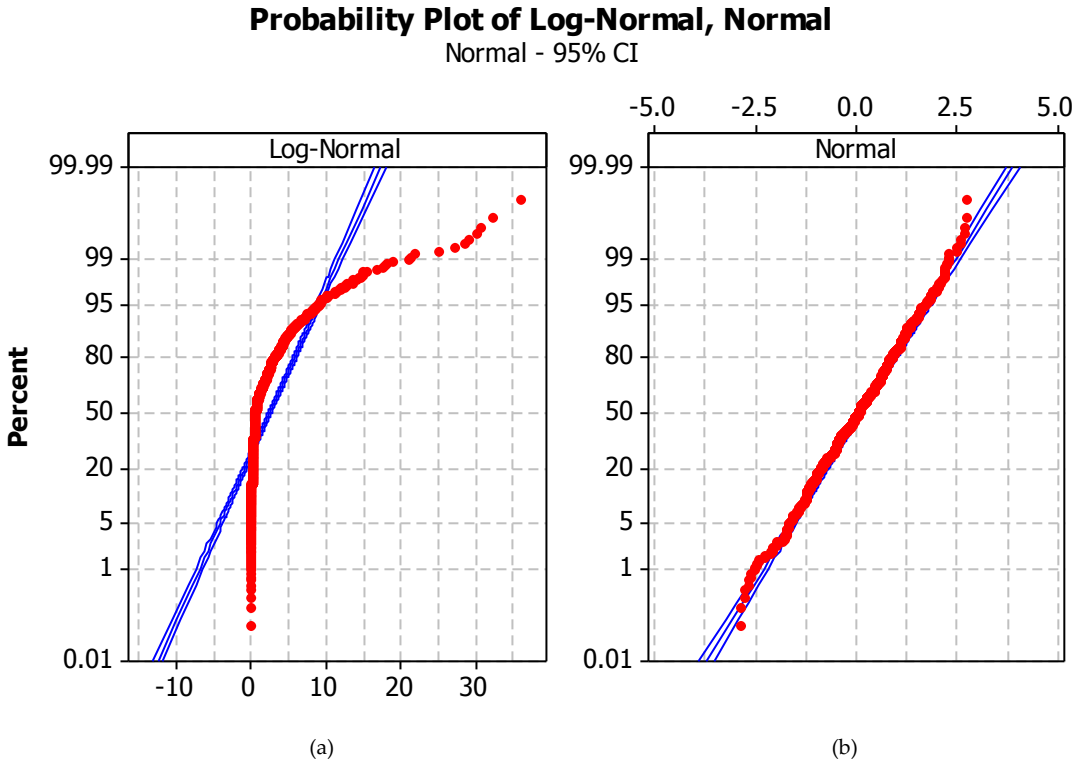

Figure 6.4: Example output from Minitab v16.1.1: Probability plots of (a) a random non-normal data set (in this case, a log-normal one) (b) a normally distributed data set.

The Y-axis indicates the cumulative normal probability (as a % in this case) vs. the observed probability. When the expected probability falls on the theoretical (normal) probability (and on a straight line for this type of plot), the data set can be

considered to follow a normal distribution. In figure 6.4 (b), this is the case: the red dots are data points, whilst the middle blue line, indicates the expected values for the normal distribution. The adjacent two blue lines indicate the 95% confidence interval for the normal probability plot. Figure 6.4 (a) shows substantial deviation from normality (in this case, a simple log-normal data set was chosen as an example – any non-normal dataset would do to serve as an example).

Figure 6.5 shows the results from Minitab for the data presented in Figure 6.1:

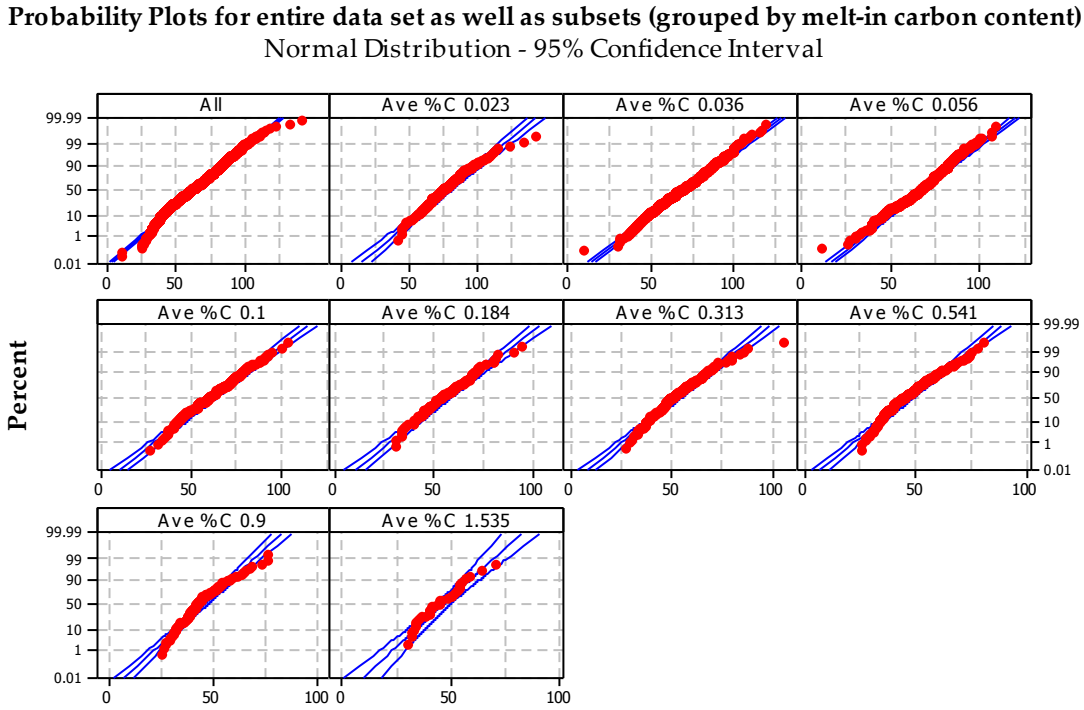

Figure 6.5: Cumulative probability plots for the entire dataset (labeled "All"), as well as each subset of data points (for each of the chosen melt-in carbon content values). The *x* variable is the tap nitrogen content.

Figure 6.5 shows the probability plots for the entire data set (based on the data in Figure 6.1), with each subset (based on the chosen groupings of the melt-in carbon analyses) as well. There is slight deviation from normality, especially for lower nitrogen contents (in this case sub-40ppm), which should not impact the results significantly, since nitrogen levels in an EAF, practically, are highly unlikely to be below 50 ppm (i.e. reported values below 50 ppm probably reflect some error in the analyses). The individual subsets also show normality, with slight deviations at higher (e.g. 0.9% and 1.535%) C levels, which might be attributed to the limited number of analyses available for these subsets of data.
To confirm that the data are approximately normally distributed, the Anderson-Darling Test for Goodness of Fit was employed (using Minitab v16 and EasyFit v5.5).

The Anderson-Darling Statistic is a general test to compare whether a specific data set conforms to an expected cumulative distribution function – in this case, the test

was used to evaluate whether or not each of the subsets conform to a normal distribution. Detailed discussion of this common test is beyond the scope of this dissertation – it was merely used to confirm the normal probability plots.

The following hypothesis test was performed, using the Anderson-Darling Statistic (denoted, AD):

The null and alternative hypothesis:

H_0: the data set is not significantly different from a normal data set;
H_A: the data set is significantly different from a normal data set.

The confidence level of 95% (α=0.05) was set for this test.
The critical value for rejection / acceptance was calculated as **2.5018** (EasyFit 5.5 software does this automatically).

Therefore: To accept the null hypothesis (i.e. that, with 95% confidence the observed data does not differ significantly from a normal distribution), the Anderson-Darling Statistic should be less than the critical value of **2.5018.**

Table 6.1 shows the results from the EasyFit 5.5 software package:

Table 6.1: Descriptive Statistics from EasyFit/Minitab for the subsets of data

	Average (%C)									
	0.023	**0.036**	**0.056**	**0.1**	**0.184**	**0.313**	**0.541**	**0.9**	**1.535**	**Overall**
Mean	78.22	70.91	67.48	62.31	56.68	52.97	47.31	44.78	45.53	64.59
Standard Deviation	17.4	15.44	13.94	14.18	12.63	12.25	11.05	10.25	9.863	16.93
Number of points	181	1128	780	245	151	215	238	144	38	3127
AD	0.613	0.906	2.741	0.417	0.312	1.142	1.626	2.221	0.507	4.227
Critical Value	2.5018									
Reject H_0 ?	No	No	Yes[1]	No	No	No	No	No	No	

Notes: 1. This subset of data was rejected as a normal distribution (for an average melt-in carbon content of 0.056%), although the AD-value is close to the critical value. One disadvantage of the Anderson-Darling test is that it weights the tail values higher than other tests, likely leading to this rejection – if one eliminates sub 40ppm N data (a mere 4 data points) from this dataset of 780 observations, it is easily accepted, hence the data set was accepted as normal within practical limits.

With the subsets of data shown to be approximately normal (for all practical purposes), one can now draw a new set of curves, which illustrate, again, the importance of the melt-in carbon content on the final nitrogen content of the melt at tap. This is illustrated in Figure 6.6. This figure allows the plant to predict the probability of meeting a given nitrogen specification, based on the melt-in carbon content.

The probability (Fig 6.6) was calculated using the probability density function for a normal distribution (since the mean and standard deviation is now known); in MS Excel, this is simply a value easily returned using the NORMDIST() function.

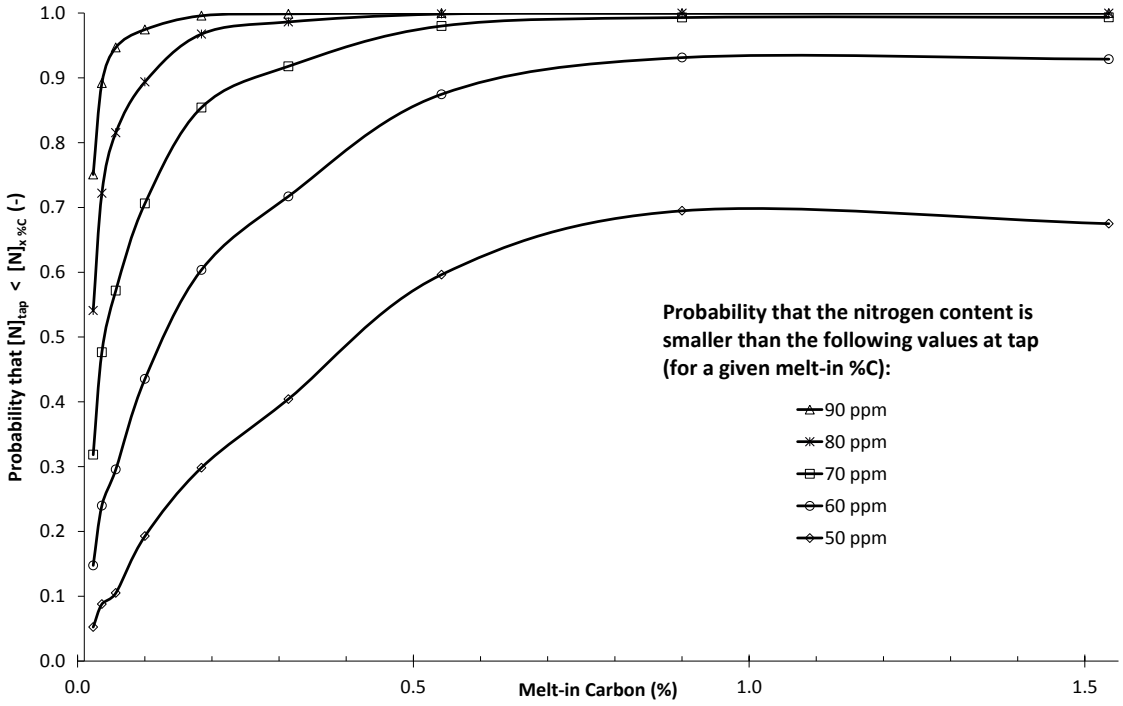

Figure 6.6: The probability, for a given melt-in carbon content, that the tap nitrogen will be below a certain level in an EAF charging DRI , hot metal and scrap as feed.

If one considers a melt-in carbon content of 0.3%, the probability that the nitrogen content at tap would be less than 80 ppm is 98.6%. Since the aim tap nitrogen at the plant in question is as low as possible (yet sub 80 ppm levels are acceptable), this is a very important number to keep in mind, when the furnace operator starts the melt-in process. For the lowest group of melt-in carbon contents (average carbon content 0.023%) the probability of achieving 80 ppm tap nitrogen or less is only 54%; this probability increases to 89% with a melt-in carbon content of 0.1%.

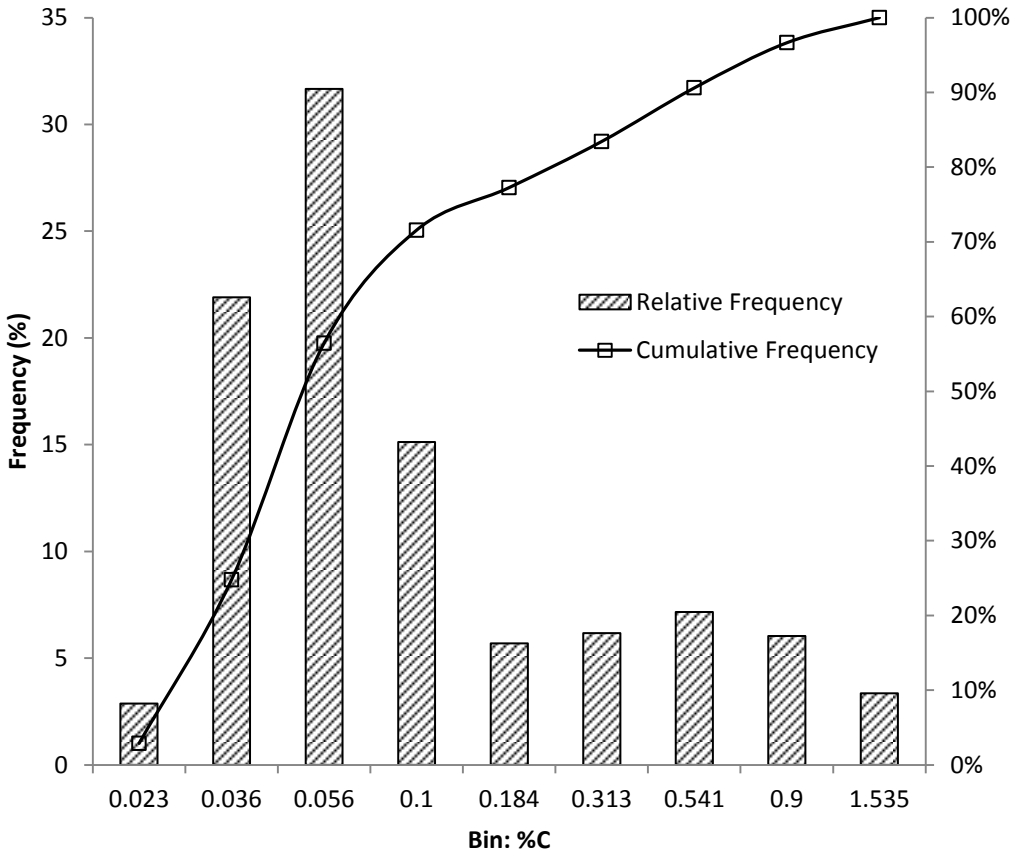

Figure 6.7: Histogram of the melt-in carbon analyses for three EAFs (see Figure 6.1)

In conclusion: Figure 6.7, a histogram of the amount of melt-in carbon, shows that the melt-in carbon content is most frequently below 0.3%. This is consistent with the observation that the tap nitrogen content is generally high.

Chapter 7:
Nitrogen Control in Electric Steelmaking: Conclusions, Proposed solutions and Recommendations for further research

7.1. Conclusion and Main Findings

The main findings of this project were:

1. Direct reduced iron produced in SL/RN rotary kilns can cause nitrogen pick-up in electric furnace steelmaking. In contrast to DRI produced in other processes (where gaseous reductants are used and the DRI is carburized), SL/RN DRI does not contribute to lower tap nitrogen levels: not by dilution, nor by "carbon boil" (since SL/RN DRI contains virtually no carbon). Quantitative results are shown in Chapter 4 of this dissertation.

2. Dissolved nitrogen is present in SL/RN DRI (on average more than 90 ppm, depending on particle size as shown in Chapter 4). The most plausible process step where nitriding of DRI particles occurs, is within the first section (first 10% of the length of the unit) of the rotary cooler (which follows the reduction step in the rotary kiln) where a gaseous atmosphere of N_2-CO_2 is in contact with solid DRI at high temperature (approximately 1000°C) (Fe is present as austenite at this temperature and readily dissolves up to 185 ppm of N).

3. Kinetic analysis shows that it is feasible for DRI particles to pick up nitrogen in the "nitriding-zone" of the rotary cooler which is the first section which is lined with refractory material. A kinetic model for each possible rate-determining step, shows that bulk gas flow, solids mixing in the cooler, pore diffusion and solid state diffusion are all rapid processes, for nitriding of DRI particles (See Chapter 5). The most plausible rate limiting step is that of nitrogen dissociation on the iron surface, which can be even further retarded by the presence of sulphur.

4. A strong relationship was found between the melt-in carbon content of the bath and the nitrogen content of the liquid steel at tap. Statistical analysis of plant data shows that the nitrogen content of liquid steel produced in an electric arc furnace process can be controlled to meet the requirement that it be lower than 80 ppm, if the melt-in carbon content of the steel bath is at least 0.3% C (Chapter 6).

7.2. Proposed solutions

To achieve the required melt-in carbon content, the carbon should be preferably charged into the basket. There have been suggestions of carburising DRI at the plant, to increase the carbon content thereof – but this option is unlikely to be effective, since most of the DRI is charged through the roof of the furnace. Goldstein and Fruehan[55] showed that in order to realise the benefits of carbon in DRI, it cannot be charged through the roof after slag has formed – the low density of DRI (DRI density ranges[42] from 1.5-4 t/m^3 – SL/RN DRI has a density of[42] ca. 1.6 t/m^3, which is lower than that of slag – typically 2-3 t/m^3) does not allow for deep penetration required for removal of nitrogen from a steel melt.

Goldstein and Fruehan[55] studied the mechanism by which DRI reduces nitrogen in steel in laboratory experiments with DRI but found that the evolution of CO happens in the slag phase and hence, the principle of the removal of nitrogen by DRI is one of simple dilution. They further tested the efficiency of nitrogen removal by bubbling CO gas through a steel melt and found that nitrogen is removed much quicker by this method. This is apparent from the slopes of the graphs in Fig 7.1.

Briquetting of SL/RN DRI can also be done, as showed by Sibankin[42]- approximate pressure of 350 MPa during briquetting can provided a maximum density of around 5 t/m^3; this would be dense enough to penetrate the slag layer, provided the briquettes are large enough as well, to have enough momentum to fall through the slag layer and penetrate the melt. In this case, the carburization of DRI would also be necessary if an increase in melt carbon is to be obtained.

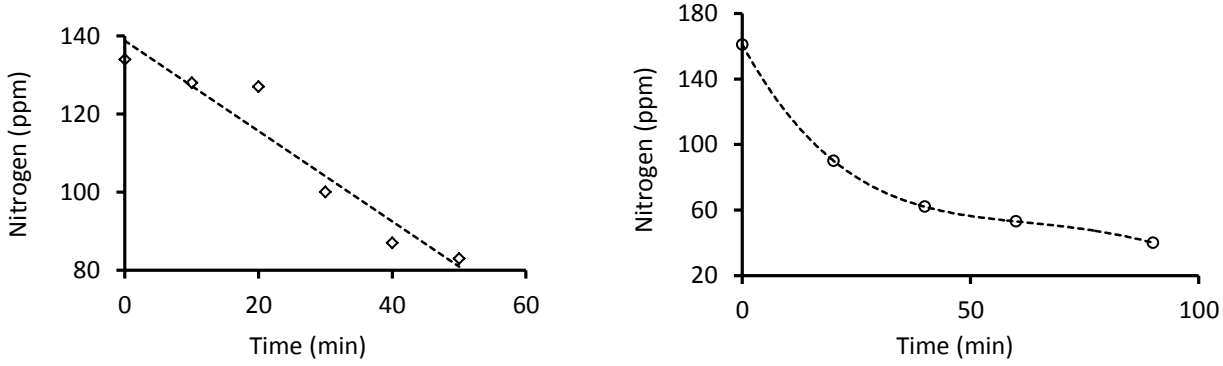

Figure 7.1: The addition of DRI (Pellets made from MIDREX DRI with 1.61% C) to a steel melt reduced the nitrogen content by (a) simple dilution and (b) bubbling CO gas through a steel melt reduced nitrogen faster (Goldstein & Fruehan[55]).

Based on this argument, carburization of DRI (which implies setting up a carburizing system at the plant, which could work with, for example, use coke oven gas) would not necessarily benefit the EAF steelmaking process, unless the DRI is charged with the basket (it should be noted that even then carbon would tend to react with FeO ion the DRI, releasing CO before melting).

In contrast, the role of carbon boil in removing nitrogen is well established, and supported by the strong role of melt-in carbon demonstrated in this work. Pilliod[56] showed plant data (see Figure 7.2) that illustrate the large decrease in nitrogen during the carbon boil period ("E" in Figure 7.2), and stated that a minimum of 0.3% C removal is required for adequate nitrogen removal. This value agrees with the plant data from this work, shown in Figure 6.2.

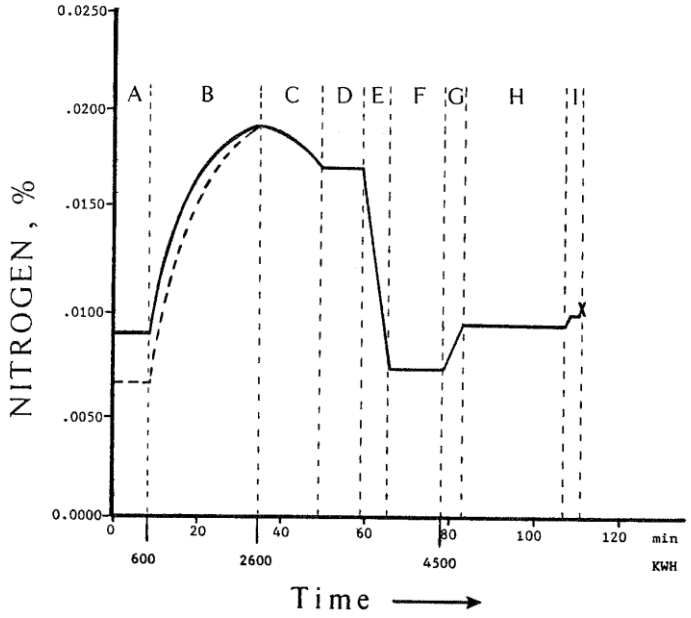

Figure 7.2: Nitrogen content during the entire steelmaking process. (A: Electrodes boring through a cold charge, B: Small molten pool forms and grows with #1 tap; C: Remaining charge melted with #2 tap; D: Bath heated to carbon boil temperature; E: Carbon boil period; F: Ferroalloy additions made and bath heated to tapping temperature; G: Tapping)[56].

7.3. Recommendations for further work

Following the argument by Goldstein and Fruehan[55] it does not seem that carburizing DRI would solve the problem on the plant. Focus should be on briquetting of DRI, with the addition of a carburizing agent (such as coke breeze, readily available on the plant) to some of the DRI and to subsequently charge this into the basket, to ensure that the melt-in carbon content is achieved. Furthermore, the amount of carbon should also be sufficient to compensate for all of the unreacted FeO present within DRI. Current practice of charging anthracite fines should be evaluated, since the oxidation of carbon when it is charged results in some losses, resulting in the low melt-in carbon level. Ideally, an investigation should be done where the plant engineer tests the yield of carbon from a specific carburizing agent – with enough data, it can be determined how to, on an economical basis, ensure that the melt-in carbon content is above 0.3%.

Appendix 1

A.1. Rate of penetration of nitrogen gas into the solids bed, if it were static (using the "Dusty-Gas" model by Tien and Turkdogan.

For nitriding of the metallic iron to occur, gaseous nitrogen needs to diffuse into the solids bed (in the rotary kiln or cooler), against the outward flow of carbon monoxide (which is the main gaseous product of the reduction reaction. A simplified static one-dimensional situation was considered (for this step), to test the basic concept that diffusion of nitrogen into the solids bed is feasible under kiln and cooler conditions.

The approach of Tien and Turkdogan[57], developed to assess the diffusion of inert gas into metal oxide/carbon mixtures during reduction, was adapted for this purpose. Tien and Turkdogan derived the relevant relationships from the "dusty gas model"; the relationships relevant to diffusion in CO-N_2 mixtures (where the two diffusing species have the same molar mass and hence diffuse at the same rate) are as given below:

The total flux (due to diffusion and bulk gas flow) in the z direction is as follows:

$$J_i = -D_e \frac{dn_i}{dz} - X_i \frac{\kappa P}{\mu RT} \frac{dP}{dz} \qquad \text{(A.1.1)}$$

where D_e is the effective diffusion coefficient through the pores of the solids bed, dn_i/dz is the concentration gradient, X_i is the mole fraction (note that $n_i = X_i P/RT$), κ is the permeability of the solids bed, P the absolute pressure, μ is the gas viscosity, R the ideal gas constant and T the absolute temperature.

The shape of the concentration profile into the solids bed would depend on the relative efficiency of diffusion into the solids bed, and uptake of nitrogen by the iron (through pore diffusion, and diffusion of atomic nitrogen into the austenite). A first estimate of the concentration profile in the solids bed can be obtained by assuming stagnant diffusion of nitrogen, that is, $J_{N_2} = 0$. This would be the case if nitrogen uptake by the iron (rather than diffusion into the bed) is rate-determining. For this case, the flux of carbon monoxide out of the bed is then given by[57]:

$$J_{CO} = -\frac{1}{RT}\left(D_e + \frac{\kappa P}{\mu}\right)\frac{dP}{dz} \qquad \text{(A.1.2)}$$

This relationship was applied to a one-dimensional static bed containing iron oxide, iron and carbon, which is undergoing reduction. The temperature was assumed to

be uniform within the mixture (as is the case in the bed in the SL/RN kiln[58]), and hence the rate of reaction was assumed to be the same everywhere within the solids bed, generating CO at a rate of $\dot{N}_V$ mol/m³s (per unit volume of bed). The solids bed was bounded below by an impervious surface, with the upper surface exposed to the nitrogen-containing gas freeboard (see Figure A.1.1).

For this situation, the flux of CO (in the z direction) depends on position within the bed, as follows:

$$J_{CO} = -\dot{N}_V (h - z) \qquad \text{(A.1.3)}$$

If it is assumed that the pressure change within the reacting bed is small compared with the total (absolute) pressure, the relative pressure within the bed is found as follows, by integration:

$$\Delta P = \dot{N}_V \frac{RT}{D_e + \frac{\kappa P}{\mu}} \left(zh - z^2/2 \right) \qquad \text{(A.1.4)}$$

The local (steady-state) concentration of N_2 for stagnant diffusion is found from the flux equation, for J_{N_2}=0:

$$D_e \frac{dX_{N_2}}{dz} \frac{P}{RT} = -X_{N_2} \frac{\kappa P}{\mu RT} \frac{dP}{dz}; \quad \frac{dX_{N_2}}{dz} = -X_{N_2} \frac{\kappa}{\mu D_e} \frac{dP}{dz}$$

$$\text{Substition of the expression for } \frac{dP}{dz} \text{ then yields:}$$

$$X_{N_2} = X^{o}_{N_2} \exp\left[-\frac{\kappa RT \dot{N}_v}{D_e \mu (D_e + \kappa P/\mu)} \left(zh - z^2/2 \right) \right] = X^{o}_{N_2} \exp\left[-\frac{\kappa}{D_e \mu} \Delta P \right] \qquad \text{(A.1.5)}$$

where $X°_{N_2}$ is the mole fraction of nitrogen in the gas freeboard at the surface of the solids bed.

The following input data were used to evaluate the nitrogen concentration:

The binary diffusivity (in CO-N_2 mixtures) was calculated from the equation of Hirschfelder et al[59,60] Following Tien and Turkdogan[57] it was assumed that the Knudsen diffusion effect is negligible; hence the effective diffusivity through the pores of the solids bed is given by:

$$D_e = \frac{\varepsilon}{\tau} D_{12} \qquad \text{(A.1.6)}$$

where ε is the void fraction in the solids bed, τ the tortuosity, and D_{12} the binary diffusivity. The void fraction was assumed to be approximately 0.4; the tortuosity

was estimated from the expression given by Wu et al.[61], giving τ=1.69, or ε/τ=0.24, which appears reasonable.[62] Gas viscosity was similarly calculated from the Hirschfelder et al.[59,60] correlations, using the values for carbon monoxide.

The permeability was calculated from the Kozeny-Carman equation,[62] assuming spherical particles:

$$\kappa = \frac{d_p^2 \varepsilon^3}{150(1-\varepsilon)^2} \qquad \text{(A.1.7)}$$

where d_P is the particle diameter. In the calculations a particle diameter of 0.01 m was assumed (the 80% passing size of particles is 9.5 mm on average). (While the predicted pressure drop depends strongly on the particle diameter, the mole fraction of nitrogen within the solids bed was not found to be a strong function of d_P.)

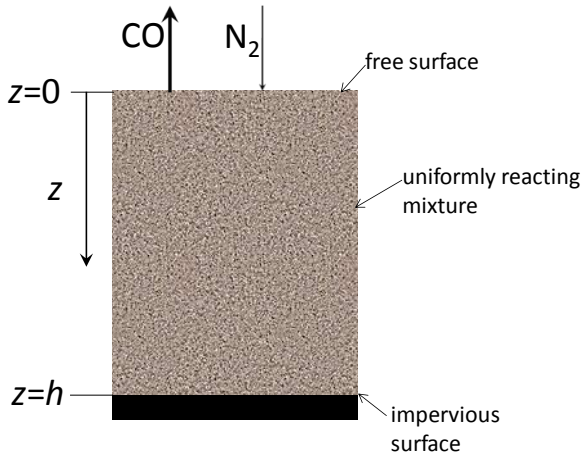

Figure A.1.1: Schematic drawing of the physical situation considered for the dusty-gas calculations.

Ranges of CO generation rate ($\dot{N}_V$) which could be expected under industrial conditions were estimated from the results of Venkateswaran and Brimacombe,[58] for the Griffith kiln (length 125 m, internal diameter 5.5 m). The reduction profile (as reproduced in Figure A.1.2) was used to calculate the reduction rate at different positions in the kiln, using the following values from Venkateswaran and Brimacombe:[58] a degree of fill of 0.2, Fe feed rate of 1036 t/day (based on a pellet feed rate of 1570 t/day, and an assumed pellet Fe content of 66%), a molar ratio of O to Fe in the pellets of 1.5, and a concentration of Fe in the solids bed of 763 kg/m^3. As the figure shows, the CO generation rate peaks at approximately 1.6 mol/m^{3}s, and decreases to approximately one-tenth this value towards the discharge end. In the rotary cooler, the CO generation rate would be even lower, as the temperature drops and CO formation (through reaction of CO_2 with the coal) slows. Hence three CO generation rates were considered: 1 mol/m^{3}s (representative of the main reduction zone at the centre of the kiln), 0.1 mol/m^{3}s (representative of the conditions towards the discharge end of the kiln), and 0.01 mol/m^{3}s (assumed to be representative of conditions in the cooler). The bed temperature was taken to be 1000°C in the kiln, and 900°C in the cooler (it was found that the calculated nitrogen concentration profile changes little if the assumed temperature changes). The nitrogen content of the gas at the bed surface was taken to be 65% (corresponding to full combustion of pure CO with air). The ambient pressure was taken to be 1 atm.

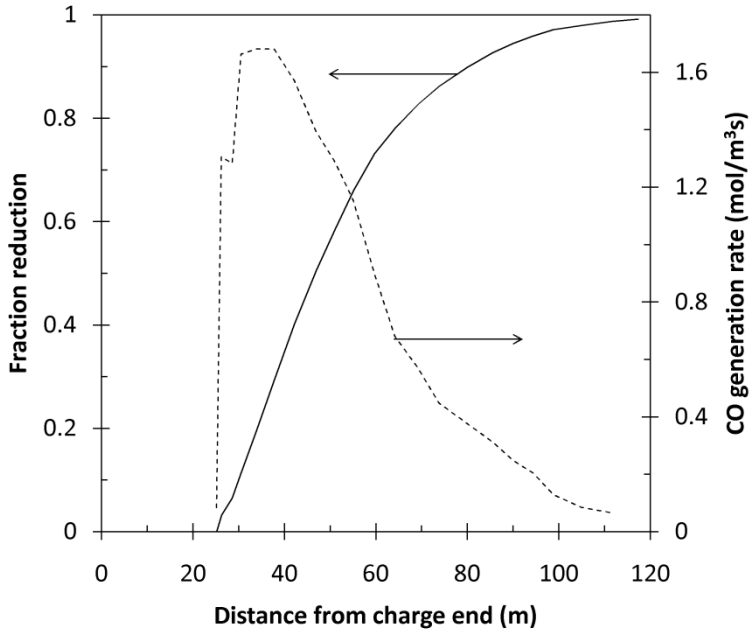

Figure A1.2: Reduction profile as reported by Venkateswaran and Brimacombe[58], with the volumetric generation rate of CO as calculated from these data.

The bed depth (*h* in Figure A.1.1) was taken to be half the maximum depth of the bed in the rotary kiln (since the bed in the kiln is in the shape of a circular segment, its depth varies from zero up to a maximum depth of 1.4 m, for the Griffith kiln).

The results presented in Figure A.1.3 shows that essentially no nitrogen penetration into the solids bed is predicted in the centre of the kiln (where the reaction rate is high), with some penetration towards the kiln exit, and significant penetration in the cooler. The pressure increase within the bed can be seen to be affected mainly by the reaction rate, and secondarily by the temperature difference between the kiln and cooler.

As a measure of the degree of nitrogen penetration, the position within the bed was determined where the partial pressure of nitrogen in the gas phase would be in equilibrium with 50 ppm of dissolved nitrogen in the austenite, based on the literature values for nitrogen solubility[63] (the value of 50 ppm is an arbitrary one, but chosen to reflect a significant nitrogen pick-up). Based on this criterion, the depth of nitrogen penetration into the solids bed at the centre of the kiln is estimated to be 2.2 mm (that is, less than the diameter of the solid particles), compared with 22 mm towards the kiln exit, and 267 mm in the cooler. These values emphasise that the nitrogen penetration depth is approximately inversely proportional to the CO generation rate, and that significant nitrogen penetration is expected close to the kiln exit, and certainly in the rotary cooler.

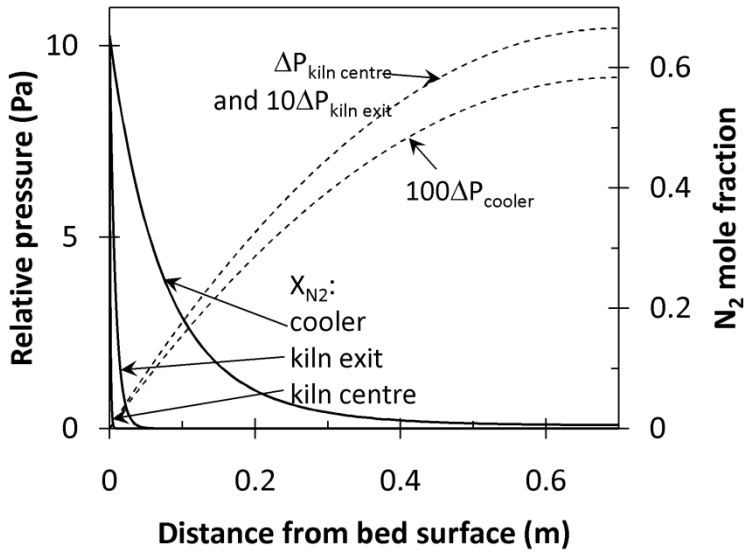

Figure A.1.3: Calculated pressured drop (broken lines; pressure drop for kiln exit and cooler multiplied by 10 and 100 respectively to show these on the same graph) and nitrogen mole fraction, within the solids bed at different positions in the SL/RN process.

A.2. Data used to evaluate the diffusion distance (L) for solid-state nitriding

Particles of different sizes were used to determine the width of the DRI "arms". Particles from different size fractions were used to test whether there was a significant difference in arm width for small and large particles. Measurements were made around the edges of the particle, as well as in the middle.

Table A.2.1: Measured values of the DRI "arm" width (microns).

-13.2+9.5 mm size fraction				-5.6+2.0 mm size fraction			
Edge		*Middle*		*Edge*		*Middle*	
Mean	22.74	Mean	20.62	Mean	13.42	Mean	21.78
Standard Error	0.64	Standard Error	0.51	Standard Error	0.58	Standard Error	1.21
Median	22.75	Median	19.82	Median	10.46	Median	15.09
Mode	29.02	Mode	17.85	Mode	5.43	Mode	11.49
Standard Deviation	7.43	Standard Deviation	7.77	Standard Deviation	12.61	Standard Deviation	18.29
Sample Variance	55.19	Sample Variance	60.36	Sample Variance	159.01	Sample Variance	334.35
Count	133	Count	235	Count	471	Count	228
Confidence Level(95.0%)	1.27	Confidence Level(95.0%)	1.00	Confidence Level(95.0%)	1.14	Confidence Level(95.0%)	2.39

References

1. J. Kopfle and R. Hunter: "Direct reduction's role in the world steel industry." *Ironmaking and Steelmaking*, vol. 35, no. 4, pp. 254-289 (2008).

2. World Steel Dynamics: "2010 World Direct Reduction Statistics." from www.midrex.com (Accessed, 30 June 2011).

3. http://www.worldsteel.org/statistics/DRI-production.html (Accessed, 6 June 2013)

4. W.C. Leslie: "The Physical Metallurgy of Steels", McGraw-Hill, 1981, pp. 68,70,74,78,79,83,88.

5. D.T. Llewellyn, "Nitrogen in steels.", *Ironmaking and Steelmaking*, vol. 20,no. 1, pp. 35-41 (1993).

6. W.B. Morrison, "Nitrogen in the steel product.", *Ironmaking and Steelmaking*, vol. 16, no. 2, pp. 123-128 (1989).

7. B. Chamont, P. Chemelle and H. Biausser: "Nitrures D'Aluminium et Ductilité à Chaud des Aciers Coulés en Continu.", *Proceedings of the international symposium on Simulation of Welding, Hot Forming and Continuous casting"*, May 2-4, 1988, Ottawa, Canada, pp. vol II 48-52.

8. N.H. Croft, "Solubility model to predict effects of aluminium and nitrogen contents on susceptibility of steel castings to intergranular embrittlement.", *Metals Technology*, vol. 10, pp. 285-290 (August, 1983).

9. K.O. Bazaleeva: "Mechanisms of the influence of Nitrogen on the structure and properties of steels (a review).", *Metal Science and Heat Treatment*, vol. 47, nos. 9-10, pp. 455-461 (2005).

10. G.K. Sigworth and J.F. Elliott: "The thermodynamics of liquid dilute iron alloys." *Metal Science*, vol. 8, pp. 298-310 (1974).

11. J. Siwka: "Equilibrium constants and nitrogen in liquid metals and iron alloys." *ISIJ International*, vol. 48, pp. 385-394 (2008).

12. F. Oeters: "The Metallurgy of Steelmaking", Cambridge : Woodhead Publishing, p. 168 (1989).

13. E.T. Turkdogan: "Fundamentals of Steelmaking", The Institute of Metals, Cambridge University Press, pp. 38-39, 77-79, 97, 255 (1996).

14. R.J. Fruehan: "Ladle Metallurgy Principles and Practices", The Iron and Steel Society, Inc, pp. 17, 42.

15. M. Byrne and G.R. Belton: "Studies of the Interfacial Kinetics of the Reaction of Nitrogen with Liquid Iorn by the ^{15}N-^{14}N Isotope Exchange Reaction", *Metallurgical Transactions B,* vol. 14B, pp. 441-449 (1983).

16. R.J. Fruehan and L.J. Martonik: "The Rate of Absorption of Nitrogen into Liquid Iron Containing Oxygen and Sulfur.", *Metallurgical Transactions B,* vol. 11B, pp. 615-621 (1980).

17. J.D. Katz and T.B. King: "The kinetics of nitrogen absorption and desorption from a plasma arc by molten iron." *Metallurgical Transactions Series B*, vol. 20B, pp. 175-185 (1989).

18. K. Mundra and T. Debroy: "A general model for partitioning of gases between a metal and its plasma environment." *Metallurgical Transactions Series B*, vol. 26B, pp. 149-157 (1995).

19. R.J. Fruehan, B. Lally and P.C. Glaws: "A model for nitrogen absorption in steelmaking processes." *Transactions of the ISS, Iron &Steelmaker*, vol. 14, pp. 31-36 (1987).

20. N. Bannenberg, B. Bergmann and H. Gaye: "Combined decrease of sulphur, nitrogen, hydrogen and total oxygen in only one steelmaking operation." *Steel research*, vol. 63, pp. 431-437 (1992).

21. Personal communication, Y. Rolla, ArcelorMittal (Vanderbijlpark plant).

22. K. Suzuki, K. Kitamura, T. Takenouchi, M. Funazaki and Y. Iwanami: "Manufacturing of high-purity steels by ladle refining." *Transactions of the ISS, Iron & Steelmaker*, vol. 9, pp. 33-37 (1982).

23. D. Trotter, D. Varcoe, R. Reeves and S. Hornby Anderson: "Use of HBI and DRI for Nitrogen Control in Steel Products.", *SEAISI Quaterly (Malaysia)*, Vol. 31, No. 2, pp. 39-50 (April, 2002).

24. Y. Zhang and R.J. Fruehan: "Effect of the bubble size and chemical reactions on slag foaming." *Metallurgical and Materials Transactions B*, vol. 26B, no. 4, pp. 803-812 (1995).

25. S.S. Ghag, P.C. Hayes and H. Lee: "Model development of slag foaming." *ISIJ International*, vol. 38, no. 11, pp. 1208-1215 (1998).

26. K. Ito and R.J. Fruehan: "Study on the Foaming of CaO-SiO2-FeO slags: Part I. Foaming Parameters and Experimental Results." *Metallurgical and Materials Transactions B,* vol. 20B, no. 4, pp. 509-514 (1989).

27. K. Ito and R.J. Fruehan: "Study on the Foaming of CaO-SiO2-FeO slags: Part II. Dimensional Analysis and Foaming in Iron and Steelmaking Processes." *Metallurgical and Materials Transactions B,* vol. 20B, no. 4, pp. 509-514 (1989).

28. E.B. Pretorius and R.C. Carlisle: "Foamy Slag Fundamentals and Their Practical Application to Electric Furnace Steelmaking." *Iron and Steelmaker,* vol. 26, no. 10, pp. 79-88 (1999).

29. O.P. Jha, S.N. Sinha and A. Chatterjee: "The Role of Foamy Slags in Steelmaking."*Transactions of the Indian Institute of Metallurgy,* vol. 48, no. 2, pp. 107-113 (1995).

30. F.-Z. Ji, K.S. Coley and G.A. Irons: "Carbon Injections Kinetics and Slag Foaming in EAF Slags." *15th IAS Steelmaking Conference,* San Nicolas, Argentina, pp.13-22 (2005).

31. D.L. Schroeder: "The Advantages of Foaming Slag Control in EAF Operation." *Steel Times,* vol. 225, no. 10, pp. 368-369 (2000).

32. H. Sun, K. Gao, V. Sahajwalla, K. Mori and R.D. Pehlke: "Kinetics of Gas Oxidation of Liquid Fe-C-S Alloyes and Carbon Boil Phenomenon." *ISIJ International,* vol. 39, no. 11, pp. 1125-1133 (1999).

33. K. Gao, V. Sahajwalla, H. Sun, C. Wheatly and R. Dry: "Influence of Sulfur Content and Temperature on the Carbon Boil and CO Generation in Fe-C-S Drops." *ISIJ International,* vol. 40, no. 4, pp. 301-308 (2000).

34. M.S. Lee, D.J. Trimble and L.J. Wibberley: "Evaluation of low-grade iron carbide as a reagent for enhanced nitrogen desorption in steel melts." *Scandinavian Journal of Metallurgy*, vol. 30, no. 3, pp. 121-126 (2001).

35. J. Ruer: "Production and use of iron carbide for the EAF." *Steel times*, vol. 225, no. 3, pp. 114-116 (1996).

36. P.J. Koros, "A Practical Example of the Benefits of Carbon in HBI and DRI", *AISTech 2005 Proceedings*, Vol. 1, Charlotte, North Carolina, USA, 9-12 May 2005, pp. 395-402.

37. D. Anghelina, G.A. Irons and G.A. Brooks, "Nitrogen Removal from Steel by DRI Fines Injection", *AISTech 2005 Proceedings*, Vol. 1, Charlotte, North Carolina, USA, 9-12 May 2005, pp.403-412.

38. T.M. Scarnati, I. Alvarez and F.L. Sammt, "Chapter 9: Use of DRI in Steelmaking", Direct Reduced Iron: Technology and Economics of Production and Use, Iron and Steel Society of AIME, 1980, Chapter republished in 1999, pp. 127-145.

39. J.A.T. Jones, "Alternative Feedstocks for EAF Steelmaking: Value In Use", *Electric Furnace Conference Proceedings*, pp. 457-478 (1998).

40. B. Anameric and S.K. Kawatra: "Properties and features of Direct Reduced Iron", *Mineral Processing and Extractive Metallurgy Review,* vol. 28, pp. 59-116 (2007).

41. B. Strohmeier and W. Peters, "Operation of large UHP-arc furnaces with kiln based DRI at Iscor Ltd.", *Metallurgical Plant Technology*, 6 (1986).

42. J.G. Sibakin: "Development of the SL Direct Reduction Process", *General Meeting of the American Iron and Steel Institute,* New York, May 23, pp. 1-42 (1962).

43. http://energy.er.usgs.gov/products/databases/CoalQual/, Last Accessed: 31 Jul. 13

44. R. Falcon and A.J Ham: "The characteristics of Southern African coals", *Journal of the South African Institute of Mining and Metallurgy,* vol. 88, no. 5, pp. 145-161 (1988).

45. P. Abelha, I. Gulyurtlu, and I. Cabrita: "Release Of Nitrogen Precursors From Coal And Biomass Residues in a Bubbling Fluidized Bed", *Energy Fuels* 2008, vol. 22, no. 1, pp. 363–371 (2008).

46. M.D. Heydenrych, P. Greeff, A.B.M. Heesink, G.F. Versteeg.: "Mass transfer in rolling rotary kilns: a novel approach", *Chemical Engineering Science,* vol. 57, no. 18, pp. 3851-3859 (2002).

47. J.R. Ferron and D.K. Singh.: "Rotary Kiln Transport Processes", *AIChE Journal,* vol. 37, no. 5, pp. 747-758 (1991).

48. Welty, J.R, Wicks, C.E., Wilson, R.E. and Rorrer, G.: "*Fundamentals of Momentum, Heat and Mass Transfer"*, 4th ed., Wiley, p. 434, (2001).

49. H.J. Grabke: "Reaktion von Ammoniak, Stickstoff und Wasserstoff an der Oberfläche von Eisen. II. Zur Kinetik der Nitrierung von Eisen mit N_2 un der Desorption von N_2." *Berichte der Bunsengesellschaft für physikalische Chemie*, vol. 72, pp. 541-548 (1968).

50. H.J. Grabke, E.M Petersen and S.R. Srinivasan: "Influence of adsorbed sulfur on surface reaction kinetics and surface self-diffusion on iron." Surface Science, vol. 67, pp. 501-516 (1977).

51. J.A. Theron. "Swaelverdeling gedurende die direkte reduksie van ystererts". Masters Dissertation, University of Pretoria, South Africa (1986).

52. Holman, J.P. "*Heat Transfer*", 10th international ed., McGraw-Hill, pp. 673-674. (2010)

53. Bakker, H. et al. *Landolt-Börnstein Zahlenwerte und Funktionen aus Naturwissenschaften und Technik, Band 26: Diffusion in festen Metallen und Legierungen.* Herausgeber: H. Mehrer, Springer-Verlag Berlin, p. 481.

54. Thode, H.C. "*Testing For Normality"*, Volume 164 of Statistics: textbooks and monographs", Marcel-Dekker, Inc, New York, p15-40, 100.

55. D.A. Goldstein, R.J. Fruehan and B. Ozturk: "The behavior of DRI in slag-metal systems and its effect on the nitrogen content of steel." Iron & Steelmaker, vol. 26, no. 2, pp. 49-61 (1999).

56. C.F. Pilliod: “Variables affecting the nitrogen content of carbon and low alloy acid electric arc furnace steels”, *Electric Furnace Conference Proceedings*, 1988, pp. 107-110.

57. R.H. Tien and E.T. Turkdogan: "Mathematical analysis of reactions in metal oxide/carbon mixtures." *Metallurgical Transactions Series B*, vol. 8B, pp. 305-313 (1977).

58. V. Venkateswaran and J.K. Brimacombe: "Mathematical model of the SL/RN direct reduction process." *Metallurgical Transactions Series B*, vol. 8B, pp. 387-398 (1977).

59. J.O. Hirschfelder, R.B. Bird and E.L. Spotz: "The transport properties of non-polar gases." *The Journal of Chemical Physics*, vol. 16, pp. 968-981 (1948).

60. J.O. Hirschfelder, R.B. Bird and E.L. Spotz: "The transport properties of gases and gaseous mixtures." *Chemical Reviews*, vol. 44, pp. 205-231 (1949).

61. J. Wu, B. Yu and M. Yunj: "A resistance model for flow through porous media." *Transport in porous media*, vol. 71, pp. 331-343 (2008).

62. W.L. McCabe, J.C. Smith and P. Harriott: *Unit operations of chemical engineering*, 6th edition. McGraw-Hill, 2001. pp. 159, 858.

63. S. Ban-ya and Y. Iguchi: "½N2 (g) = N (α-, γ-, δ-Fe)." *Steelmaking Data Sourcebook*, revised edition, The Japan Society for the Promotion of Science, The 19th Committee on Steelmaking. Gordon and Breach Science Publishers, 1988. pp. 27-34.